



POLITECNICO

MILANO 1863

Inverted Pendulum AUTOMAD

D'Aleo Damiano
De Vecchi Alessandro
Furia Matteo
Roncoli Roberto

Politecnico di Milano



Contents

1	Introduction	1
2	Modeling	1
2.1	Assumptions and conventions	1
2.2	Dynamic model	2
2.3	System identification	4
2.3.1	Static friction identification	4
2.3.2	Cable stiffness identification	4
2.3.3	DC motor identification	5
2.3.4	Pendulum identification	8
2.3.5	Horizontal arm identification	9
2.3.6	Simulation Error Method Identification	12
2.3.7	Optimization Results	13
3	Linearized Model	14
4	Frequency Validation	15
5	Open loop analysis	17
6	Position control of the horizontal arm	19
7	Closed Loop Frequency Validation	22
8	Stabilization of the pendulum in upright position	23
8.1	Regulator	23
8.1.1	Pole Placement	23
8.1.2	Linear Quadratic Regulator	23
8.2	Observer	24
8.2.1	Filtered Derivative	24
8.2.2	Luenberger Observer	24
8.2.3	Kalman Filter	25
8.2.4	Comparison between observers	26
8.3	Final results	27
8.3.1	Comparison of α	27
8.3.2	Comparison of V_m	28
9	Position control and stabilization in upright configuration	29
9.1	Extended Pole Placement	29
9.2	Extended LQR	29
9.3	Frequency validation	30
9.4	Results comparison	32
9.4.1	Comparison of θ	32
9.4.2	Comparison of α	32
9.4.3	Comparison of V_m	33
9.5	Robustness test	34
9.6	Comments	34
10	Swing up	35
10.1	Switching system and results	36
11	Extended Kalman Filter	37



12 Finite Horizon Optimal Control Problem	38
13 Appendix	41

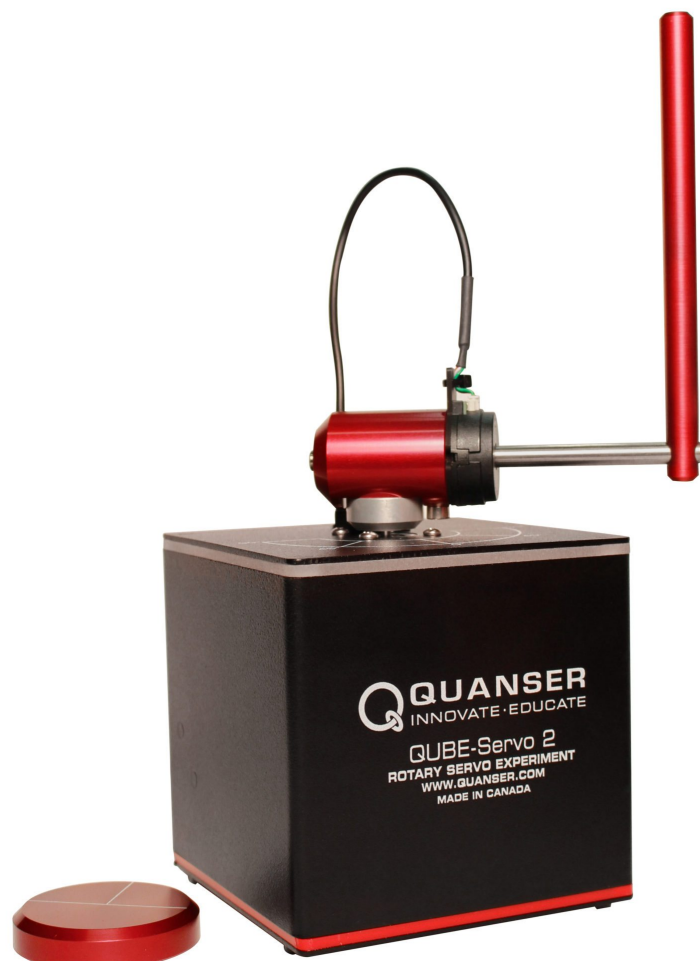


Figure 1: QUBE-Servo 2 setup



1 Introduction

The inverted pendulum is a non linear under actuated mechanical system which is unstable in the upright position. It has just one control action which is the voltage provided to a DC servo motor and two degrees of freedom that are the rotational angle of the horizontal arm θ and of the pendulum α ; such angles are measured through two optical incremental encoders.

Our goals in the laboratory activity are:

1. Position control of the horizontal arm.
2. Stabilization of the pendulum in the upright position.
3. Position control of the horizontal rod while keeping the pendulum in the upright configuration.
4. Swing up of the vertical arm.

2 Modeling

2.1 Assumptions and conventions

Before entering the details of the mathematical model, few assumptions have been made to simplify the treatise.

1. The motor and the horizontal arm are rigidly coupled.
2. The horizontal arm and the pendulum are two rigid links.
3. Only viscous damping and static friction on θ have been considered.
4. The coordinate axes of the rod and pendulum are the principal axes so that the inertia tensors are diagonal.
5. The two links are long and thin so in the slender hypothesis the moments of inertia along the axes of the links are negligible [see definition of inertia tensors later on].
6. The pendulum link has rotational symmetry so the moments of inertia in two of the principal axes are equal.
7. The c.o.m of the pendulum link is at half its length.
8. The cable of the α encoder is modeled as a linear torsional spring.

The following conventions have been adopted in the model:

1. θ is assumed positive in ccw direction when viewed from above.
2. α is assumed positive in ccw direction when viewed from the front.
3. α is zero in the downward position.
4. Rest position of the spring is in $\theta = 0$.

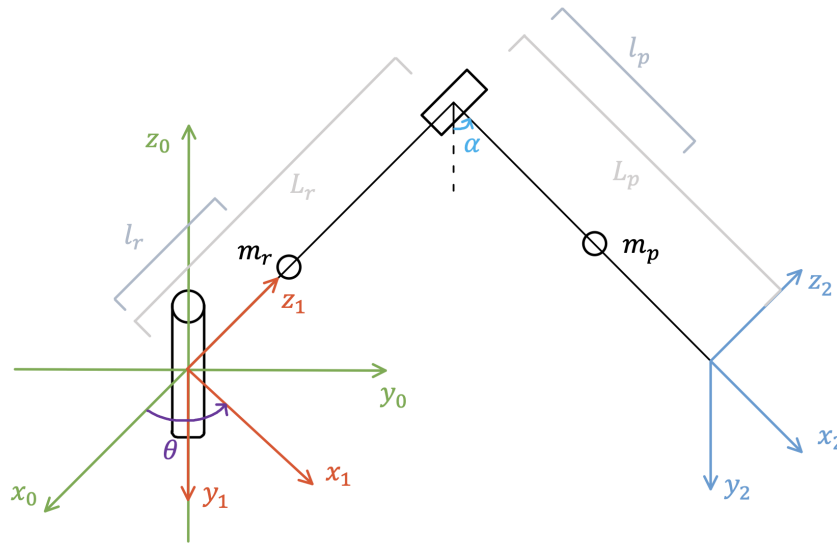


Figure 2: Model of the system at hand

2.2 Dynamic model

In order to describe the set-up, a white box approach, based on physics and mechanical principles, has been adopted called the Euler-Lagrange method.

This modelling procedure is based on the kinetic and potential energy of the links which compose our system and the general expression is:

$$\frac{d}{dt} \left(\frac{\partial L}{\partial \dot{q}_i} \right) - \frac{\partial L}{\partial q_i} = \xi_i \quad i = 1, 2$$

Where:

$$L(q, \dot{q}) = T(q, \dot{q}) - U(q) \quad q = \begin{pmatrix} \theta \\ \alpha \end{pmatrix}$$

The system can be seen as a robotic manipulator with two links and two rotational joints; as a consequence, the modelling computation has been developed as usually done in robotics through positional and rotational jacobians. At the end, a system of two differential equations is obtained:

$$B(q)\ddot{q} + C(q, \dot{q})\dot{q} + B_v\dot{q} + \tau_s + K(q - q_0) + g(q) = \tau$$

Where the inertia matrix is:

$$B(q) = m_r J_p^r J_p^r + J_o^T R_r I_r R_r^T J_o^r + m_p J_p^p J_p^p + J_o^p R_p I_p R_p^T J_o^p$$

Here it's clear the importance of the assumption of considering the inertia tensor as a matrix and not as a scalar so as to gather all possible coupled effects between the horizontal arm and the pendulum dynamics. Thanks to this, in the final model there will be all the moments of inertia referred to the pivot points of the two links and not with respect to their c.o.m..



So said, the inertia tensor matrices are:

$$I_r^r \begin{bmatrix} J_r & 0 & 0 \\ 0 & J_r + J_m + J_h & 0 \\ 0 & 0 & 0 \end{bmatrix} \quad I_p^p \begin{bmatrix} 0 & 0 & 0 \\ 0 & J_p & 0 \\ 0 & 0 & J_p \end{bmatrix}$$

The final expression of the inertia matrix is:

$$B(q) = \begin{bmatrix} m_r l_r^2 + J_r + J_m + J_h + m_p L_r^2 + (m_p l_p^2 + J_p) (\sin \alpha)^2 & m_p l_p L_r \cos \alpha \\ m_p l_p L_r \cos \alpha & m_p l_p^2 + J_p \end{bmatrix}$$

The Coriolis effects matrix $C(q, \dot{q})$ is computed using the Christoffel symbols:

$$c_{ijk} = \frac{1}{2} \left(\frac{\partial b_{ij}}{\partial \dot{q}_k} + \frac{\partial b_{ik}}{\partial \dot{q}_j} - \frac{\partial b_{jk}}{\partial \dot{q}_i} \right)$$

$$C_{ij} = \sum_{k=1}^2 c_{ijk} \dot{q}_k$$

$$C(q, \dot{q}) = \begin{bmatrix} (m_p l_p^2 + J_p) \sin \alpha \cos \alpha \dot{\alpha} & (m_p l_p^2 + J_p) \sin \alpha \cos \alpha \dot{\theta} - m_p l_p L_r \sin \alpha \dot{\alpha} \\ -(m_p l_p^2 + J_p) \sin \alpha \cos \alpha \dot{\theta} & 0 \end{bmatrix}$$

The remaining elements of the system of differential equations are:

$$g(q) = \begin{pmatrix} -m_r g_0^T J_{p_r}^r - m_p g_0^T J_{p_r}^p \\ m_r g_0^T J_{p_p}^r - m_p g_0^T J_{p_p}^p \end{pmatrix} = \begin{pmatrix} 0 \\ m_p l_p g_0 \sin \alpha \end{pmatrix}$$

$$K = \begin{bmatrix} K_s & 0 \\ 0 & 0 \end{bmatrix}$$

$$B_v = \begin{bmatrix} B_r & 0 \\ 0 & B_p \end{bmatrix}$$

$$\tau = \begin{bmatrix} \left(\frac{k_m}{R_m} V_m - \frac{k_m^2}{R_m} \dot{\theta} \right) \\ 0 \end{bmatrix}$$

$$\tau_s = \begin{bmatrix} \tau_{s_\theta} & 0 \\ 0 & 0 \end{bmatrix}$$

Finally, the complete model is:

$$\begin{cases} (m_r l_r^2 + J_r + J_m + J_h + m_p L_r^2 + (m_p l_p^2 + J_p) (\sin \alpha)^2) \ddot{\theta} + (m_p l_p L_r \cos \alpha) \ddot{\alpha} + 2 (m_p l_p^2 + J_p) \sin \alpha \cos \alpha \dot{\theta} \dot{\alpha} \\ - (m_p l_p L_r) \sin \alpha \dot{\alpha}^2 + \left(B_r + \frac{K_m^2}{R_m} \right) \dot{\theta} + \tau_{s_\theta} + K_s (\theta - 0) = \frac{K_m}{R_m} V_m \\ (m_p l_p L_r \cos \alpha) \ddot{\theta} + (m_p l_p^2 + J_p) \ddot{\alpha} - (m_p l_p^2 + J_p) \sin \alpha \cos \alpha \dot{\theta}^2 + B_p \dot{\alpha} + m_p l_p g_0 \sin \alpha = 0 \end{cases}$$

2.3 System identification

In order to have a good representation of the real system it's important to identify those parameters which are not easily measurable like damping coefficients and moments of inertia. To do so, two strategies are shown:

1. Identification based on system's responses [*by hand* identification]
2. Identification based on simulation error method via optimization [*SEM* identification]

Let's start with the first procedure.

Note: All simulations can be performed integrating the model equation with a sample time $T_s = 2ms$, in a similar way to what has been described in the section 2.3.6 or using Simulink.

2.3.1 Static friction identification

In order to identify the static friction coefficient $\tau_{s\theta}$, it's possible to perform an experiment: applying a voltage ramp with a slow slope (e.g $5 \cdot 10^{-3} \left[\frac{V}{s} \right]$), starting from the equilibrium condition $q = \begin{bmatrix} 0 \\ 0 \end{bmatrix}$. The Friction Winning Voltage can be estimated as the one from which the pendulum starts to move (Fig.3). In the equilibrium condition the system equation can be reduced to:

$$\tau_{s\theta} = \frac{K_m}{R_m} V_m$$

From which it can be inferred an estimate for the static friction coefficient $\tau_{s\theta} = 9.6120 \cdot 10^{-4} [Nm]$

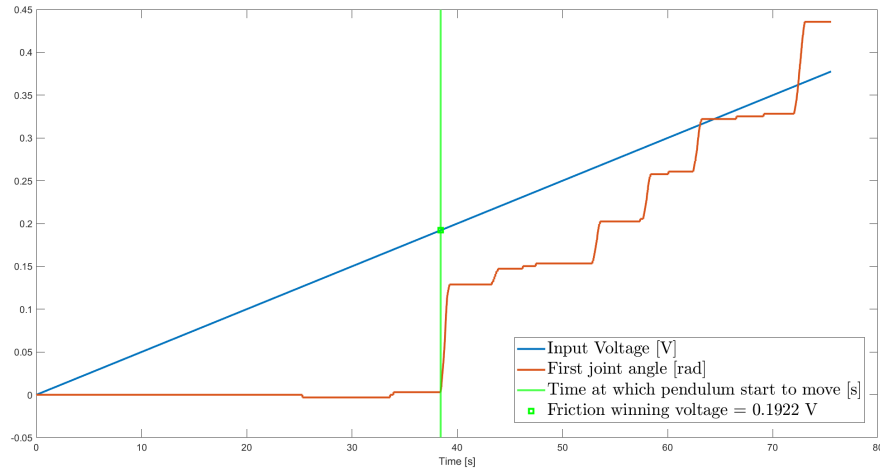


Figure 3: Static Friction Identification

2.3.2 Cable stiffness identification

Since the encoder cable is modeled as a torsional spring it makes sense to estimate its value by applying a constant voltage through a 1 V step and looking at the system equation at its stable equilibrium position $q = \begin{bmatrix} \theta_{eq} \\ 0 \end{bmatrix} \neq \begin{bmatrix} 0 \\ 0 \end{bmatrix}$.

$$K_s(\theta_{eq} - 0) + \tau_{s\theta} = \frac{K_m}{R_m} V_m$$

Looking at the measured angle from the encoder (Fig.4) it's possible to deduct that the equilibrium position is approximately $\theta_{eq} = 1.93 rad$, from which it's easy to compute $K_s = 2.6 \cdot 10^{-3} \left[\frac{Nm}{rad} \right]$

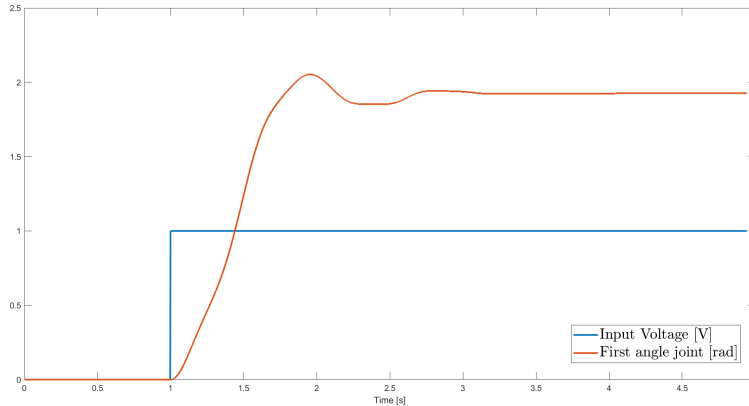


Figure 4: Cable Stiffness Identification

2.3.3 DC motor identification

Here the possibility of removing the horizontal arm and the pendulum from the set-up it's shown, so that it's possible to perform experiments on the DC motor and the attachment hub. From these experiments it's possible to identify:

1. B_r first rotational joint viscous coefficient
2. $J_m + J_h$ moment of inertia of motor rotor and attachment hub

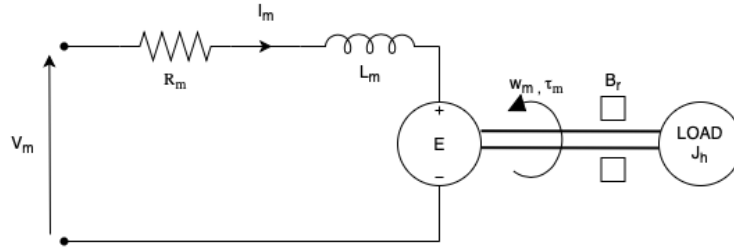


Figure 5: Servo DC motor model

The dynamic equation of a DC motor is:

$$L_m \frac{\partial I_m}{\partial t} = V_m - R_m I_m - E$$

$$E = K_m \dot{\theta}$$

Here the current's dynamics can be ignored because $L_m \ll R_m$ and the settling time of the electrical dynamics is much smaller than the sampling time of the system:

$$5 \frac{L_m}{R_m} \ll T_s$$

The complete differential equation describing the system in this identification is:

$$(J_m + J_h) \ddot{\theta} + \left(B_r + \frac{K_m^2}{R_m} \right) \dot{\theta} = \frac{K_m}{R_m} V_m$$

Then, moving to the frequency domain, writing the transfer function:

$$\frac{\theta}{V_m} = \frac{\frac{K_m}{R_m}}{s \left(J_{mh}s + \left(B_r + \frac{K_m^2}{R_m} \right) \right)}$$

It's clear that the only difference with respect to the transfer function from V_m to $\dot{\theta}$ is given by an integrator:

$$\frac{\dot{\theta}}{V_m} = \frac{\frac{K_m}{R_m}}{J_{mh}s + \left(B_r + \frac{K_m^2}{R_m} \right)}$$

Here it's performed an experiment providing the voltage V_m and collecting as output $\dot{\theta}$

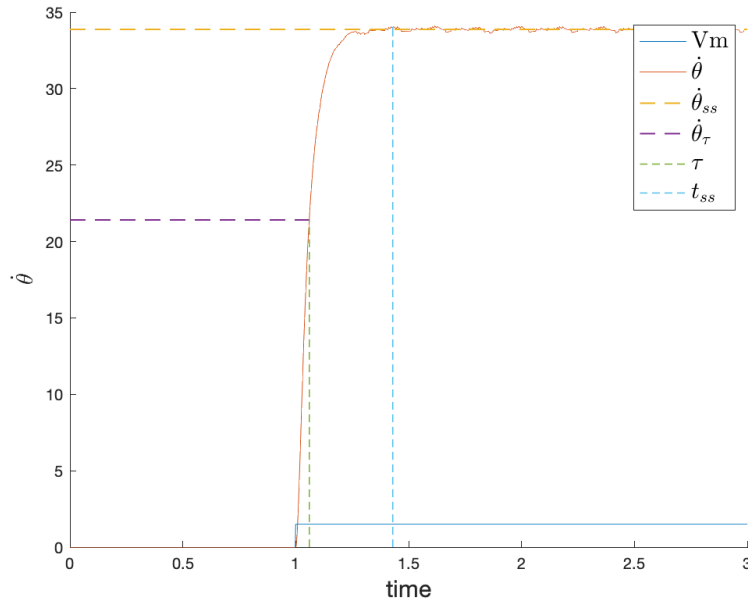


Figure 6: step 1.5V

Collecting the values of $\dot{\theta}$ at steady state and τ which is the time at which the response reaches the 63.2% of the value of $\dot{\theta}$ at steady state.

Re-writing the above mentioned transfer function as:

$$\frac{K}{1 + s\tau}$$

Here it's shown a first estimation of:

1. $B_r = 1.1521 \cdot 10^{-5} \left[\frac{Nm s}{rad} \right]$
2. $J_{mh} = 7.288 \cdot 10^{-6} \left[Kgm^2 \right]$

In the underlying figures it's clear that the values previously found are good as a validation with a step and a chirp signal has been performed.

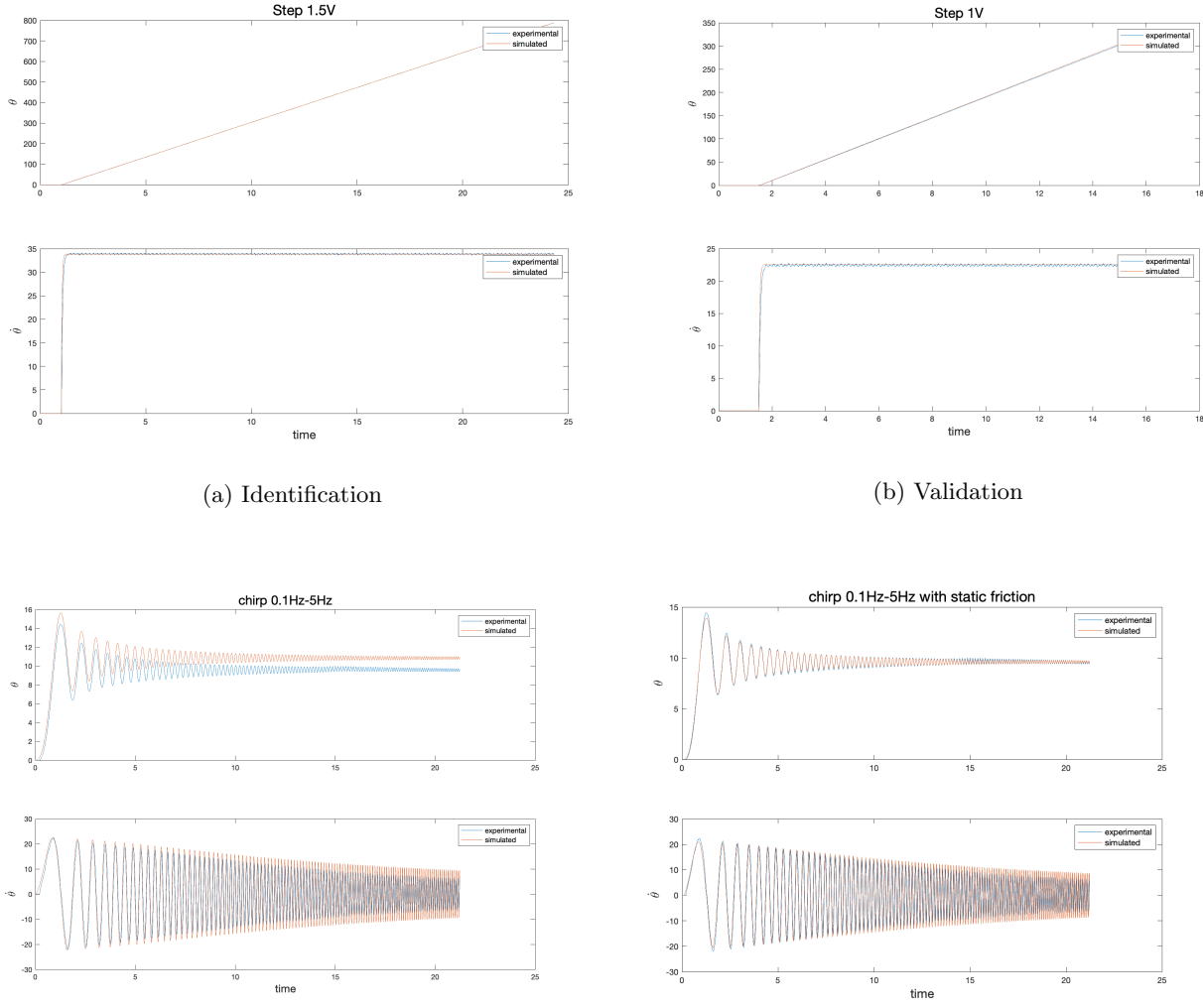


Figure 8: Validation

In the chirp validation it hasn't been possible to get a nice result because in the simulation the static friction of the motor rotor has not been modeled.

As soon as the static friction of the motor has been considered, a clearly visible better validation has been obtained. The static friction was modeled in a simple way, considering it as a dead-zone on the voltage applied in between the positive and negative value of the voltage required to win the static friction and making it work only for $\dot{\theta} \approx 0$.

2.3.4 Pendulum identification

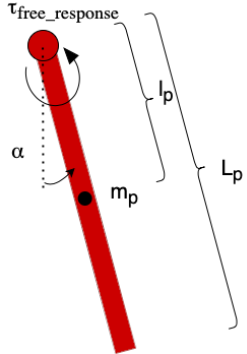


Figure 9: Frontal view of the system at hand

Immobilizing the horizontal rod allows experiencing a free response of the pendulum so that $\theta = \dot{\theta} = 0$ and $V_m = 0$. The resultant model equation representing the α dynamics is:

$$(m_p l_p^2 + J_p) \ddot{\alpha} + B_p \dot{\alpha} + m_p l_p g_0 \sin \alpha = \tau_{freeresponse}$$

For small values of α (*i.e.* $|\alpha| \leqslant 10/15^\circ$):

$$(m_p l_p^2 + J_p) \ddot{\alpha} + B_p \dot{\alpha} + m_p l_p g_0 \alpha = \tau_{freeresponse}$$

The corresponding transfer function is:

$$\frac{\alpha}{\tau_{freeresponse}} = \frac{\frac{1}{m_p l_p^2 + J_p}}{s^2 + \frac{B_p}{m_p l_p^2 + J_p} s + \frac{m_p l_p g_0}{m_p l_p^2 + J_p}}$$

After the experiment this behaviour of α has been obtained:

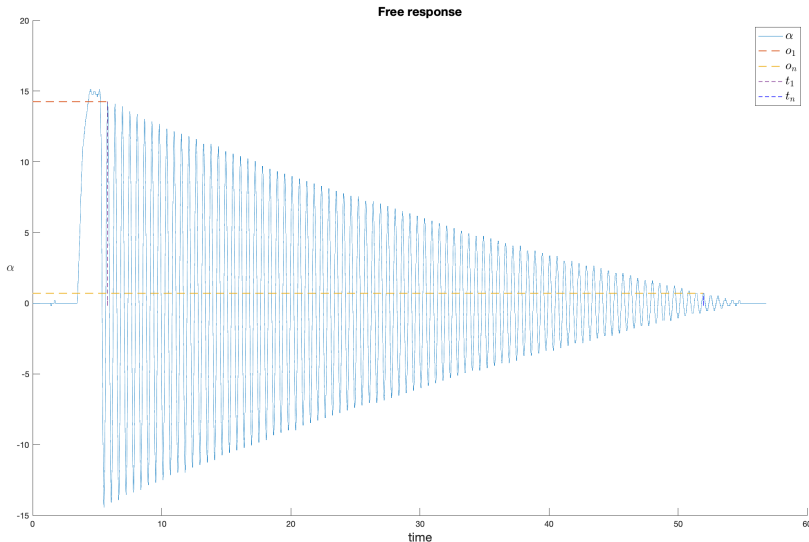


Figure 10: Free response of the pendulum



The pendulum is characterized by damped oscillations and its trend in the time domain can be described as:

$$\alpha(t) = Ae^{-\xi\omega_n t} \cos(\omega_d t - \varphi)$$

Defining:

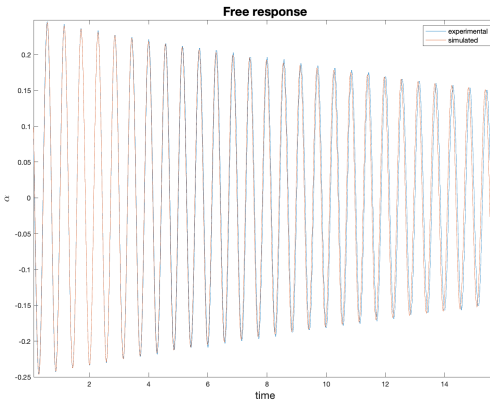
$$\begin{aligned} T_{osc} &= \frac{t_n - t_1}{n - 1} \\ \omega_d &= \frac{2\pi}{T_{osc}} \\ \xi &= \frac{1}{2\pi n} \ln \left(\frac{\alpha(t)}{\alpha(t + nT_{osc})} \right) \\ \omega_n &= \frac{\omega_d}{\sqrt{1 - \xi^2}} \end{aligned}$$

And comparing our transfer function with the general 2nd order transfer function which describes the oscillatory decaying behaviour of a dynamical system:

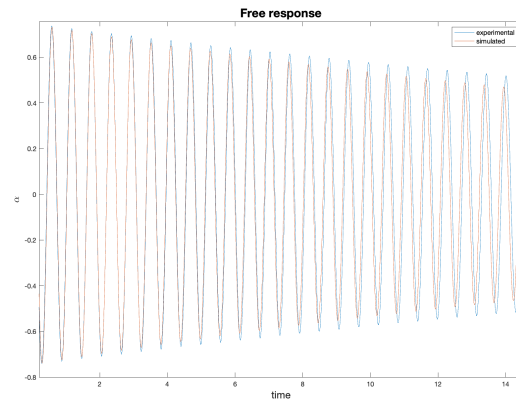
$$\frac{Y}{U} = \frac{\mu\omega_n^2}{s^2 + 2\xi\omega_n s + \omega_n^2}$$

These terms are identified:

1. $B_p = 8.0585 \cdot 10^{-6} \left[\frac{Nms}{rad} \right]$
2. $(m_p l_p^2 + J_p) = 2.4254 \cdot 10^{-5} [Kgm^2]$



(a) Identification



(b) Validation

The validation was performed on a free response experiment with a bigger initial value of α (*i.e.* $\alpha \approx 45^\circ$); therefore the previous linearization hypothesis is no more valid and for this reason it's clear that the simulated experiment does not follow precisely the real data.

2.3.5 Horizontal arm identification

In this last identification procedure, the entire system has been considered but the focus has been on the θ dynamics in order to estimate:

1. B_r , first rotational joint viscous damping coefficient

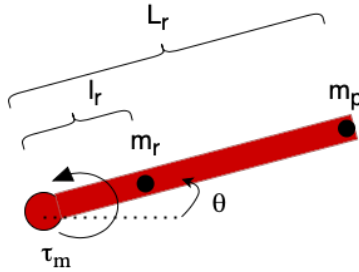


Figure 12: Top view of the system at hand

2. J_{tot} total moment of inertia seen by the motor rotor with the pendulum attached and in its downward position (pendulum in its equilibrium position)

Therefore, the dynamic equation of this procedure is like the one of the DC motor identification with the addition of the horizontal arm, the encoder cable and the pendulum (i.e. the pendulum is considered as an added mass at the end of the horizontal rod):

$$(m_r l_r^2 + J_m + J_m + J_h + m_p L_r^2) \ddot{\theta} + \left(B_r + \frac{K_m^2}{R_m} \right) \dot{\theta} + K_s (\theta - \theta_0) = \frac{K_m}{R_m} V_m$$

$$(m_r l_r^2 + J_m + J_m + J_h + m_p L_r^2) = J_{tot}$$

Keeping the angle α close to zero one can obtain the linearized model equation of the rod identification:

$$J_{tot} \ddot{\theta} + \left(B_r + \frac{K_m^2}{R_m} \right) \dot{\theta} + K_s (\theta - \theta_0) = \frac{K_m}{R_m} V_m$$

Again, moving in the frequency domain the corresponding transfer function is:

$$\frac{\theta}{V_m} = \frac{\frac{K_m}{R_m}}{J_{tot} s^2 + \left(B_r + \frac{K_m^2}{R_m} \right) s + K_s}$$

The experiment was performed giving a tiny step input to the voltage of the DC motor so that the linearized assumption of $\alpha \approx 0$ was valid. In practice, to be sure that the pendulum was not oscillating a rubber band was attached to the set-up.

The resultant plot is shown in figure 13.

Reporting one more time the general expression of the 2nd transfer function:

$$\frac{Y}{U} = \frac{\mu \omega_n^2}{s^2 + 2\xi\omega_n s + \omega_n^2}$$

Adopting these formulas :

$$\mu = \frac{\theta_{steady state}}{V_m}$$

$$M_p = \frac{\theta_{peak} - \theta_{steady state}}{\theta_{steady state}}$$

$$\xi = \sqrt{\frac{\ln(M_p)^2}{\ln(M_p)^2 + \pi^2}}$$

$$t_p = t_{max} - t_0$$

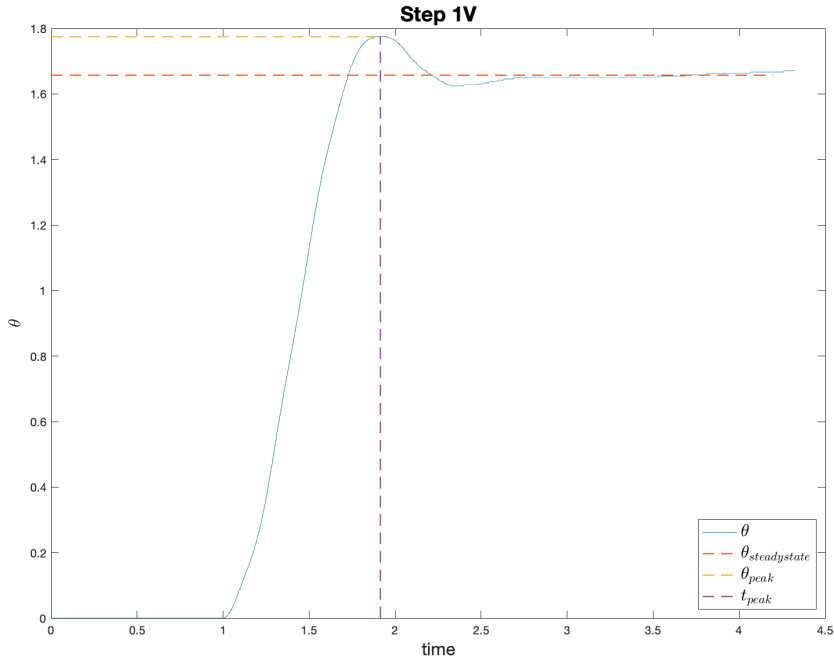
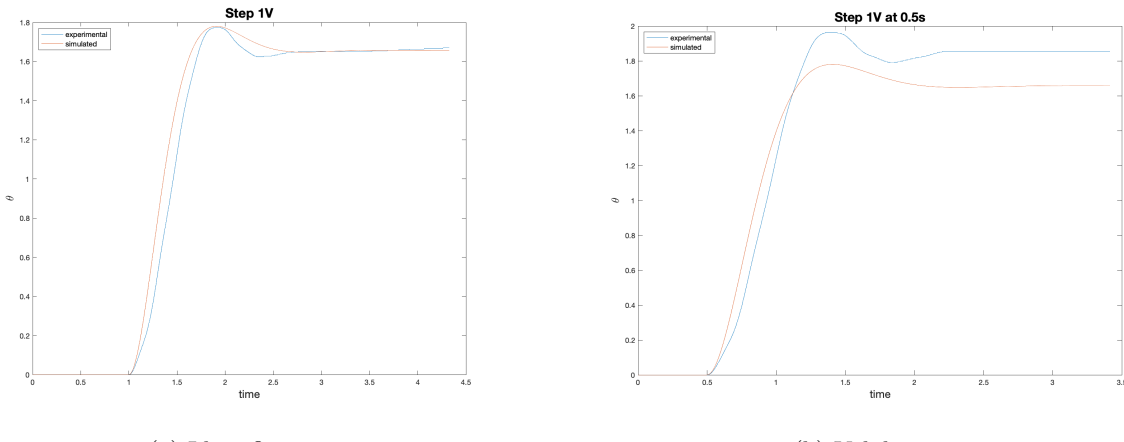


Figure 13: Step response

$$t_p = \frac{\pi}{\omega_n \sqrt{1 - \xi^2}}$$

Rearranging the previous expressions these terms have been estimated:

1. $K_s = 2.6 \cdot 10^{-3} \left[\frac{Nm}{rad} \right]$
2. $B_r = 6.4817 \cdot 10^{-4} \left[\frac{Nms}{rad} \right]$
3. $J_{tot} = 3.2352 \cdot 10^{-4} \left[Kgm^2 \right]$



As in the DC motor validation, it's not perfect due to lack of static friction modeling; implementing the same model of static friction as done in section 2.3.3 much better results have been obtained.

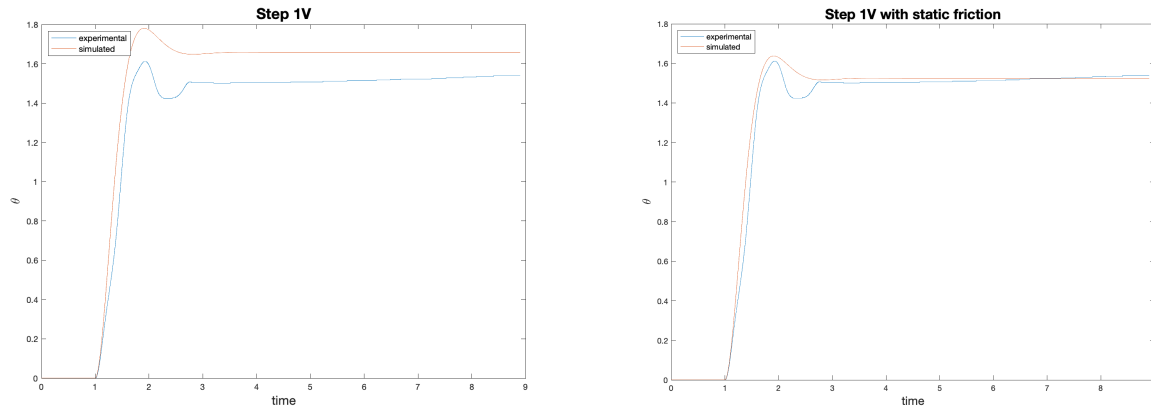


Figure 15: Validation no rubber band

2.3.6 Simulation Error Method Identification

Simulation results obtained simulating the model with the parameters identified until this section, can be improved using an optimization based method, namely SEM (Simulation Error Method), which tries to optimize the simulated response by comparing it with the measured response, through an error metric. The used solver "non linear grey identification toolbox" iteratively optimizes, via Trust-Region Reflective Gauss-Newton, the vector of parameters to reduce the error between responses. Particularly the vector of optimized parameters π is composed of:

1. Equivalent moment of inertia of the pendulum seen from the second rotational joint
2. Equivalent moment of inertia of the horizontal arm seen from the first rotational joint
3. Viscous friction coefficient of the first rotational joint
4. Viscous friction coefficient of the second rotational joint

The parameters found in the previous section were used as a warm starting of the optimization solver. This is done to guide the toolbox towards solutions that are grounded in reality and closely aligned with the previous ones.

The cost function is constructed to increase the fitting of the real-simulated pendulum angle, as well as to optimize the overall response both in frequency and time.

As it can be noticed the angle of the horizontal arm is not weighted in the cost function, this is so because in many experiments it's turned out that a shift of the angle from the zero equilibrium position is experienced due to the complex behaviour of the cable stiffness and the static friction.

While aiming to fit the response for both angles, weighting the error equally becomes problematic due to the limitations of our model equation in capturing the horizontal arm angle shift. This is detrimental to the optimization solver. Indeed while it tries to fit the response on θ drastically reduces the performance on α . This overall leads to a worse fitting on both angles with respect to considering just the error on α while minimizing the objective function.

Mathematical Formulation:

$$\min_{\pi} \sum_{i=0}^N (\alpha_{meas}(i) - \alpha_{sim}(i))^2 \quad (1a)$$

s.t.

$$\underline{\pi} \leq \pi \leq \bar{\pi}, \quad (1b)$$

$$\ddot{q} = B(q, \pi)^{-1} (\tau(v_{meas}(i)) - C(q, \dot{q}, \pi) - B_v(\pi) \dot{q} - K(\pi)(q - q_0) - g(q, \pi)) \quad (1c)$$

The parameter vector π has been constrained starting from the previous estimate found by hand, to not be too far away from it, by properly defining $\underline{\pi}$ and $\bar{\pi}$. The constraint (1c) represents the fact that the α_{sim} , is found by integrating the complete model equation. To do so the model must be reformulated with a state vector:

$$x = \begin{bmatrix} \theta \\ \alpha \\ \dot{\theta} \\ \dot{\alpha} \end{bmatrix}$$

Once done the model now is no more a 2nd order differential equation, but a 1st order one. Being so it can be integrated via Runge - Kutta 2 (chosen to compromise precision and computational complexity), with a step time $T_s = 2ms$, set like this to match the temporal discretization of the experimental setup measurements.

2.3.7 Optimization Results

The vector of optimized parameters provided by the SEM is:

$$\pi = \begin{pmatrix} J_p \\ J_{tot} \\ B_r \\ B_p \end{pmatrix} = \begin{pmatrix} 1.6469 \cdot 10^{-5} \\ 3.2818 \cdot 10^{-4} \\ 1.9485 \cdot 10^{-4} \\ 6.8412 \cdot 10^{-6} \end{pmatrix}$$

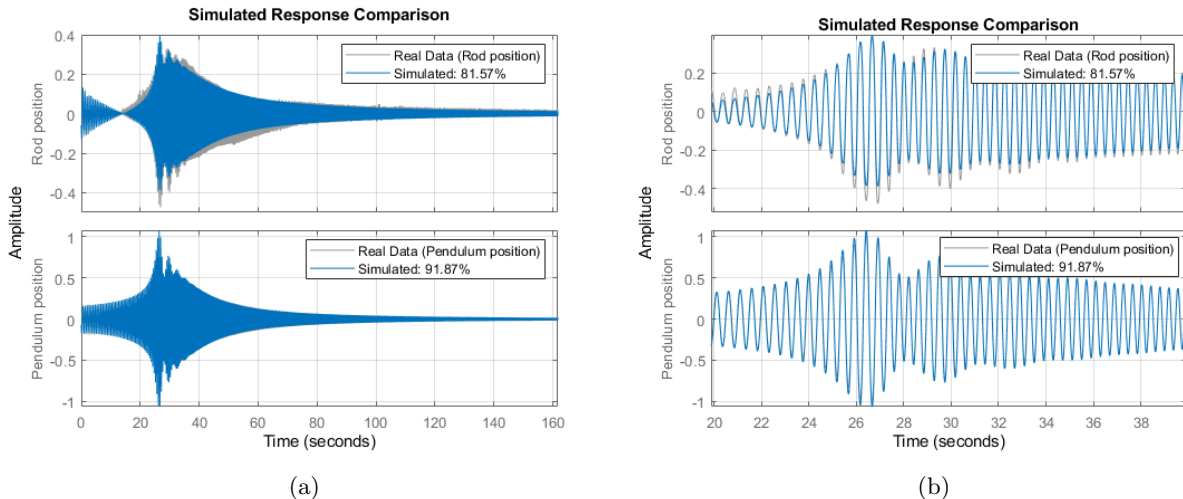


Figure 16: (a) Rod and Pendulum position Simulated VS Real Data experiment.
 (b) Zoom on resonance of (a)



3 Linearized Model

Starting from the non linear equations, and deriving by the state variables and the input what it has been obtained is this linearized set of equations around the downward position of the pendulum ($\alpha = \theta = 0$):

$$(J_{tot} + m_p L_r^2) \ddot{\theta} + (m_p l_p L_r) \ddot{\alpha} + (B_r + (\frac{K_m^2}{Rm})) \dot{\theta} + k_s \theta - (\frac{K_m}{Rm}) V_m = 0$$

$$(m_p l_p L_r) \ddot{\theta} + (m_p l_p^2 + J_p) \ddot{\alpha} + B_p \dot{\alpha} + (m_p l_p g) \alpha = 0$$

The following step is to represent the system in the “State Space Form” by defining:

$$\begin{array}{ll} x_1 = \theta & \dot{x}_1 = \dot{\theta} = x_3 \\ x_2 = \alpha & \dot{x}_2 = \dot{\alpha} = x_4 \\ x_3 = \dot{\theta} & \dot{x}_3 = \ddot{\theta} \\ x_4 = \dot{\alpha} & \dot{x}_4 = \ddot{\alpha} \end{array}$$

To simplify the model, it has been first defined this new term:

$$J_{den} = (J_{tot} + m_p L_r^2)(m_p l_p^2 + J_p) - (m_p l_p L_r)^2$$

The aim of this transformation is to obtain the system in the form:

$$\dot{\mathbf{x}} = A\mathbf{x} + B\mathbf{u}$$

Where A is a [4x4] matrix in which each term is:

$$A = \begin{bmatrix} 0 & 0 & 1 & 0 \\ 0 & 0 & 0 & 1 \\ -k_s \frac{(m_p l_p^2 + J_p)}{J_{den}} & \frac{(m_p l_p^2 L_r g)}{J_{den}} & -\frac{(B_r + (\frac{K_m^2}{Rm})) (m_p l_p^2 + J_p)}{J_{den}} & \frac{B_p m_p l_p L_r}{J_{den}} \\ k_s \frac{m_p l_p L_r}{J_{den}} & -\frac{(m_p l_p g)((J_{tot} + m_p L_r^2))}{J_{den}} & \frac{(m_p l_p^2 L_r) (B_r + (\frac{K_m^2}{Rm}))}{J_{den}} & -\frac{(B_p) (J_{tot} + m_p L_r^2)}{J_{den}} \end{bmatrix}$$

The B matrix is a [4x1] one:

$$B = \begin{bmatrix} 0 \\ 0 \\ \frac{(\frac{K_m}{Rm})(m_p l_p^2 + J_p)}{J_{den}} \\ -\frac{(\frac{K_m}{Rm})(m_2 l_2 L_1)}{J_{den}} \end{bmatrix}$$

To get the linearized model in the upward equilibrium position ($\alpha = \pi$, $\theta = 0$) the procedure is the same but the results change: the new matrices have the same structure but some terms have the opposite sign. The new matrices are:

$$A_\pi = \begin{bmatrix} 0 & 0 & 1 & 0 \\ 0 & 0 & 0 & 1 \\ -k_s \frac{(m_p l_p^2 + J_p)}{J_{den}} & \frac{(m_p l_p^2 L_r g)}{J_{den}} & \frac{(B_r + (\frac{K_m^2}{Rm})) (m_p l_p^2 + J_p)}{J_{den}} & \frac{B_p m_p l_p L_r}{J_{den}} \\ -k_s \frac{m_p l_p L_r}{J_{den}} & \frac{(m_p l_p g)((J_{tot} + m_p L_r^2))}{J_{den}} & -\frac{(m_p l_p^2 L_r) (B_r + (\frac{K_m^2}{Rm}))}{J_{den}} & -\frac{(B_p) (J_{tot} + m_p L_r^2)}{J_{den}} \end{bmatrix}$$

$$B_\pi = \begin{bmatrix} 0 \\ 0 \\ \frac{(\frac{K_m}{Rm})(m_p l_p^2 + J_p)}{J_{den}} \\ \frac{(\frac{K_m}{Rm})(m_2 l_2 L_1)}{J_{den}} \end{bmatrix}$$



4 Frequency Validation

To validate the model in the frequency domain, the *Frequency Response Theorem*, has been exploited which states that the response of an asymptotically stable system $G(s)$, when excited with a sinusoidal input with the form:

$$u(t) = A \sin(\bar{w}t + \varphi)$$

Is given by the expression:

$$y(t) = A|G(j\bar{w})| \sin(\bar{w}t + \varphi + \angle G(j\bar{w}))$$

Once understood the meaning of the theorem, is trivial to think about a way to estimate the frequency response of a linear system via experiments. In particular, the system has been subjected to 1V sinusoids at different frequencies and for each one of them the following procedure has been adopted:

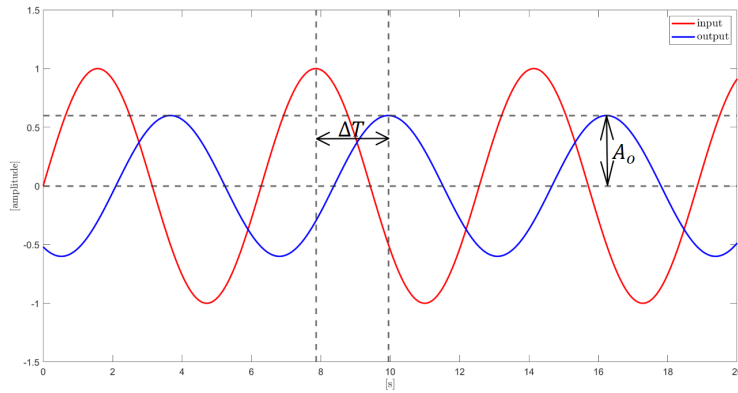


Figure 17: Input vs Output sinusoid

Experimentally measure ΔT and ΔA , then recalling that $T = \frac{1}{\bar{w}}$ and $A = 1V$ use the subsequent formulas:

$$\angle G(j\bar{w}) = \frac{2\pi}{T} \cdot \Delta T$$

$$|G(j\bar{w})| = \frac{A_o}{A}$$

Note that the measured output is not a perfect sinusoid due to noise on the measurement and non linear effects, to mitigate these factors the measurements have been taken at “steady state” (after some time) so that non linear transitory effects are less impactful.

In Fig.18, it's possible to appreciate the result of this methodology. The blue circles are the estimated frequency response using as signal the one measured from the real setup, while the red cross are the estimated frequency response using as signal the one produced with the simulator.

From this comparison it's clear that the model has been validated with success, in particular:

- The identified parameters are close enough to the real ones.
- The discrepancy on the second peak, between the model transfer function (blue line) and the estimated frequency response via experiment on the real setup (blue circle) is attributable to linearization error. In fact, the estimated frequency response estimated via experiment on the simulation (red cross) overlaps the one on the real setup as can be seen in Fig. 19

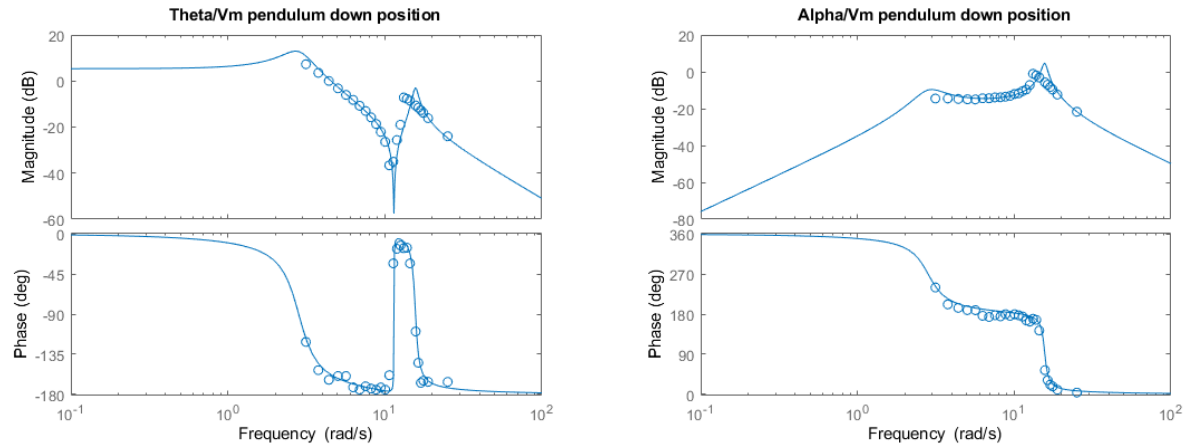


Figure 18: Validation plots (1).
 blue line = fitted model transfer function.
 blue circle = experimental frequency response using real setup

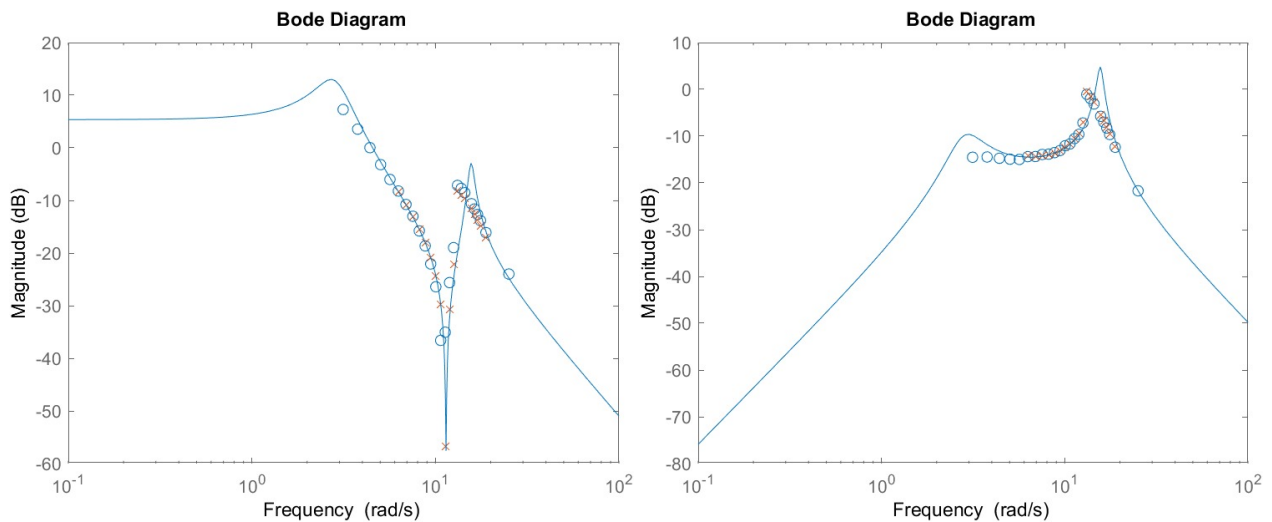


Figure 19: Validation plots (2).
 red cross = experimental frequency response using simulation



5 Open loop analysis

The system at hand is a fourth-order system with the following poles of its linearization in the downward configuration (of course, the poles of both transfer functions from the voltage input to θ and α are the same):

$$\begin{pmatrix} -0.5981 + 15.6308i \\ -0.5981 - 15.6308i \\ -0.5845 + 2.7734i \\ -0.5845 - 2.7734i \end{pmatrix}$$

All poles are in the left hand side of the real-imaginary plane so it is in an asymptotically stable equilibrium. On the other hand, the poles of the linearized system in the upright configuration are:

$$\begin{pmatrix} -15.8255 + 0.0000i \\ +14.7571 + 0.0000i \\ -0.6484 + 2.8278i \\ -0.6484 - 2.8278i \end{pmatrix}$$

A positive real pole can be immediately noticed so the upright configuration is an unstable equilibrium of the system at hand as expected.

Going back to the configuration with stable poles, it's clear that it has as dominant poles a pair of complex conjugate ones. It follows that the phase margin $\Phi \leq 75^\circ$. Indeed, the margin plot of the transfer function $V \rightarrow \theta$ is:

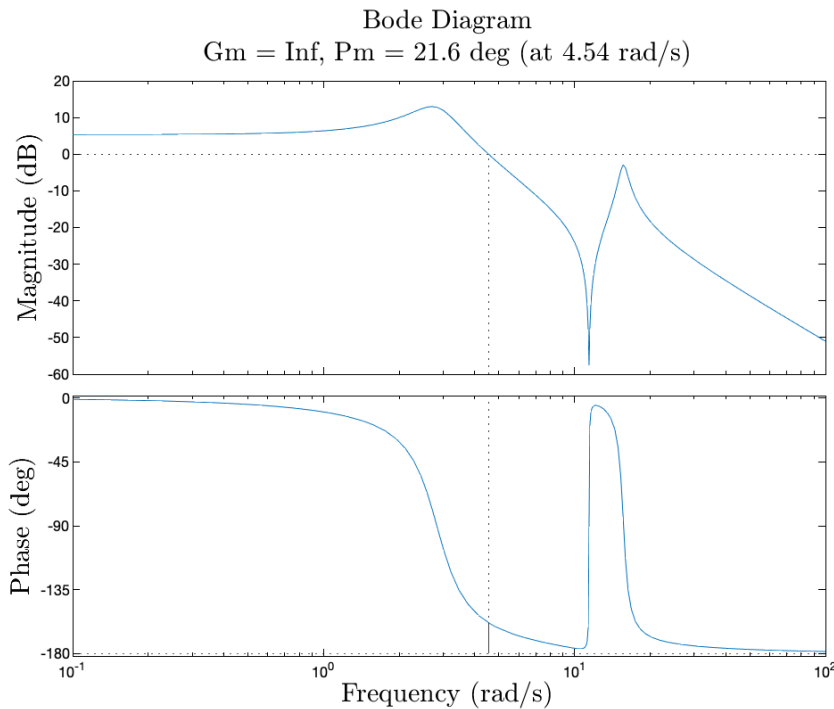


Figure 20: Margin plot $V \rightarrow \theta$ transfer function

The dominant poles can be written in general as:



$$\xi\omega_n \pm i\omega_n\sqrt{\xi^2 - 1}$$

In this case from the dominant ones, one can obtain: $\omega_n = 2.83 \frac{rad}{s}$ and $\xi = 0.206$.

From these values it's possible to acquire important features which describe the system; in fact, looking at the open loop step response and approximating the dynamic to that of the dominant poles this is obtained:

1. Peak time:

$$t_p = \frac{\pi}{\omega_n\sqrt{1-\xi^2}} = 1.13s$$

2. Settling time:

$$\frac{4.6}{\xi\omega_n} = 7.89s$$

3. Overshoot(%):

$$100e^{-\frac{\pi\xi}{\sqrt{1-\xi^2}}} = 51.6\%$$

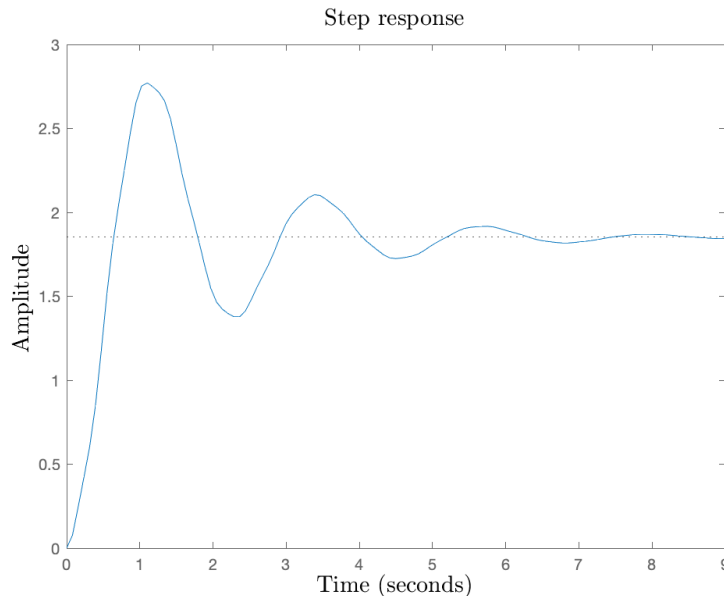


Figure 21: Simulated step response $V \rightarrow \theta$ transfer function

The presence of the overshoot is also due to the presence of two complex conjugate zeros with a real part smaller (in module) than the dominant poles' ones:

$$\begin{pmatrix} -0.0294 + 11.4262i \\ -0.0294 - 11.4262i \end{pmatrix}$$

Another interesting point is the zero analysis of the transfer function between α and V_m :

$$\begin{pmatrix} -0.0000 + 0.7921i \\ -0.0000 - 0.7921i \end{pmatrix} \cdot 10^{-7}$$

As one can see there are two zeros in the origin; this is also clear by looking at the Fig.19 where the initial slope is $+40 \frac{dB}{dec}$.



6 Position control of the horizontal arm

The aim of this section is to show how to control the angular position of the horizontal arm of the setup. Based on the previous considerations on the open loop analysis, the design choices related to specifications in *frequency domain* have been $w_c^0 = 4 \frac{\text{rad}}{\text{s}}$ and $\varphi_m^0 = 75^\circ$.

The cut-off frequency has not been chosen higher for two reasons:

1. Avoid having a very low phase margin (i.e. providing low damped oscillations in positioning).
2. Avoid the anti-resonant peak which wouldn't allow us to adopt the *Bode criterion* (i.e. the loop transfer function would cut 3 times the 0dB axis) and it wouldn't filter out the main disturbance in the position control of θ that comes from the oscillations of the pendulum.

The phase margin has been chosen high enough to have fast damped oscillations while reaching the desired θ_{ref} .

The idea is to use the PID control scheme so as to obtain the best performances. The ideal PID scheme has this form:

$$R(S) = K_p + \frac{K_i}{s} + sK_d$$

Now, knowing that $L(S) = R(S)G(S)$, we apply the *Bode criterion* through which it's possible to calculate the PID's parameters with these equations:

$$1 = |L(jw_c^0)| = |R(jw_c^0)||G(jw_c^0)| = |K_p + \frac{K_i}{jw_c^0} + (jw_c^0)K_d||G(jw_c^0)| = \sqrt{K_p^2 + \left(K_d w_c^0 - \frac{K_i}{w_c^0}\right)^2} |G(jw_c^0)|$$
$$\varphi_m^0 = 180^\circ - |\angle(L(jw_c^0))| = 180^\circ - |\angle(R(jw_c^0)) + \angle(G(jw_c^0))|$$

In the above 2 equations there are 3 unknowns: K_p, K_i, K_d . It's common norm as reported in (5), in order to have real and coincident zeros of the PID, to choose:

$$T_I = 4T_D$$

Where:

$$T_I = \frac{K_p}{K_i}$$
$$T_D = \frac{K_d}{K_p}$$

The main problem is that the ideal PID is not feasible. To overcome this issue, a real PID is implemented through this formula:

$$R(s) = K_p + \frac{K_i}{s} + \frac{sK_d}{1 + \frac{sK_d}{NK_p}}$$

$N=20$ is a constant added for feasibility with a pole in $s = -\frac{N}{T_D}$ which is far away from the frequency range of interest.

However, to avoid saturation in the control action the *Internal FeedBack Based* anti-windup scheme is used. As one can see, this scheme is a little different from the "classic one" because instead of deriving the error here it's derived directly the angle measurement to avoid a too aggressive control action. In fact if the derivative action were on the error, when there is a step change in the reference then the output of the derivative has an impulsive behavior which can saturate the voltage and bring the system away from the linear condition around which the controller has been designed.

Adopting the *IFB* scheme, the regulator can be tuned through the bode criterion, but using the following R:

$$V_m = -\frac{K_p s T_d}{1 + s \frac{T_d}{N}} \theta + \frac{1 + s T_i}{s T_i} K_p (\theta_{ref} - \theta)$$

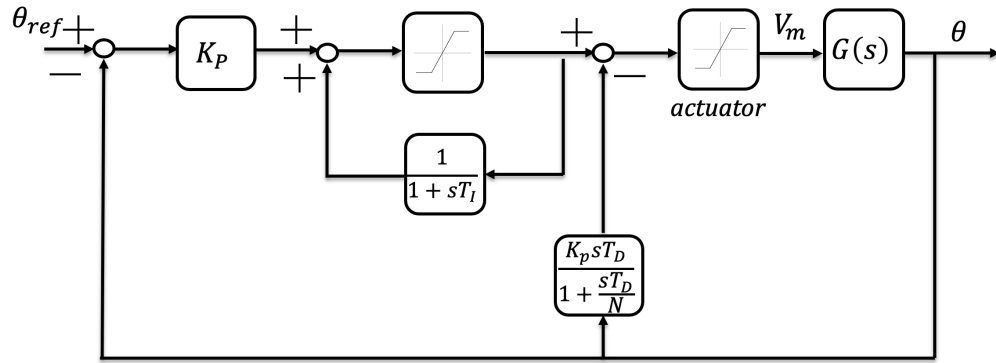


Figure 22: Final PID scheme

So the loop transfer function is:

$$\frac{\theta}{(\theta_{ref} - \theta)} = \frac{\frac{1+sT_i}{sT_i} K_p G(s)}{1 + \frac{K_p s T_d}{1 + s \frac{T_d}{N}} G(s)}$$

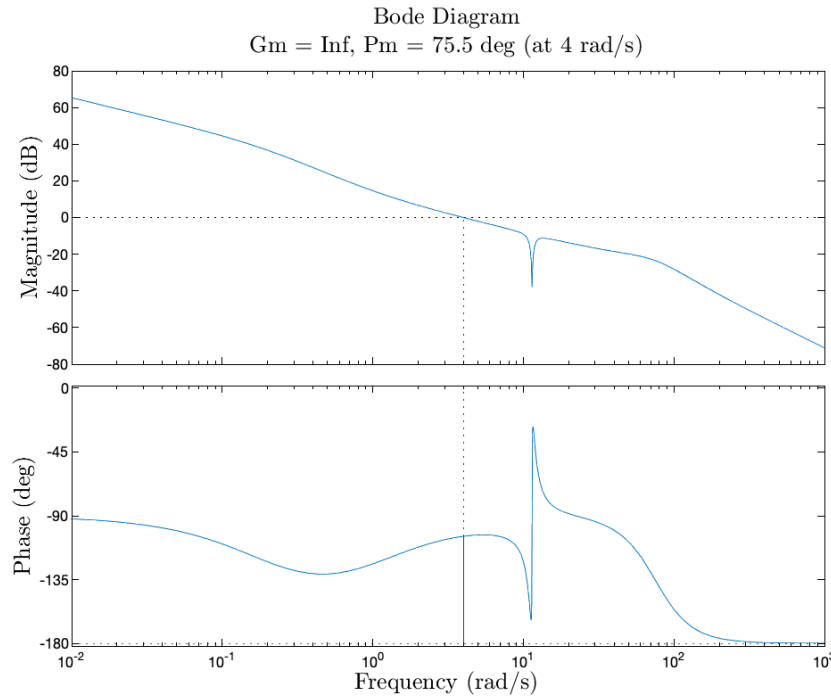


Figure 23: Bode loop transfer function

Now, looking at the resulting poles of the closed loop transfer function $F(s) = \frac{L(s)}{1+L(s)}$ it's possible to approximate it to a second order transfer function with dominant complex conjugate poles (i.e. indeed the phase margin is at 75° so the approximation to complex poles is still valid) and from those poles one can get:

$$\xi\omega_n \pm i\omega_n\sqrt{\xi^2 - 1} = -1.24 \pm 11i$$

$$t_s = \frac{4.6}{\xi\omega_n} = 3.6s$$

The settling time obtained is not too strict so as to have a smoother trajectory towards the reference and avoiding a big overshoot. A reduction of it has been tried by increasing a bit w_c^0 but it has lead to a significant rise in the overshoot peak which for fast changing reference signals can affect the tracking. As can be seen from the results, there is some overshoot which also comes from the presence of a pair of complex conjugate zeros close to the imaginary axis in the $F(s)$ transfer function:

$$(-0.0294 \pm 11.4262i)$$

The results with $K_p = 6.2, K_i = 6.3, K_d = 1.5$ are the following:

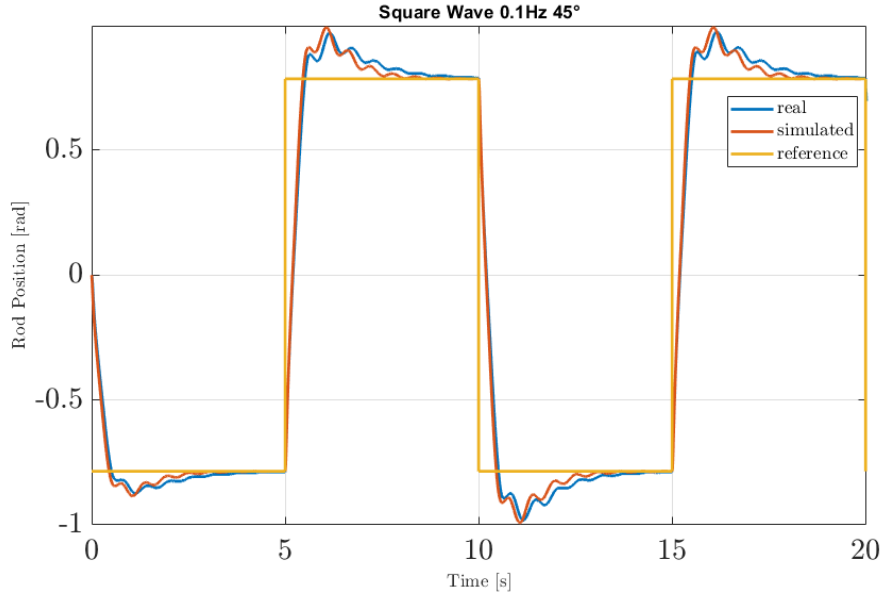


Figure 24: Square wave results

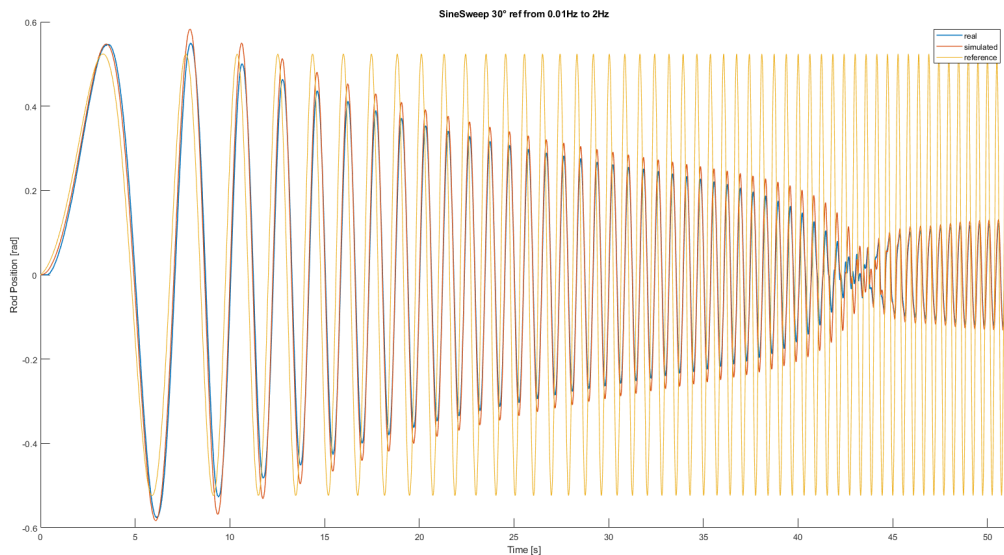


Figure 25: Sinesweep results

7 Closed Loop Frequency Validation

A different method with respect to the open loop case has been chosen to estimate the magnitude and phase from experiments, for this section and for all the following frequency validations. Considering a generic sine:

$$x(t) = A \cdot \sin(\omega_0 t + \phi)$$

Its Fourier transform is (with i as an imaginary unit):

$$X(\omega) = Ae^{-i\phi} \frac{i}{2} \delta(\omega + \omega_0) - Ae^{+i\phi} \frac{i}{2} \delta(\omega - \omega_0)$$

Given the fact that the peak of the Fourier transform is at f_0 Hz, with value corresponding to $\frac{A}{2}$ and phase $\frac{\pi}{2} + \phi_{rad}$. One can excite the system with a reference angle θ sinusoid which characteristic $A_i, \phi_i = 0, \omega_i$ are known, then decompose the spectrum of the measured signal automatically using Fast Fourier Transform to identify the frequency at which it peaks, so the one of the principal sinusoid component, and automatically retrieve the amplitude and phase of the output signal A_o, ϕ_o . So estimating the frequency response:

$$|G(i\omega_i)| = \frac{A_o}{A_i}$$

$$\angle G(i\omega_i) = \phi_o - \phi_i = \phi_0$$

The results of this procedure applied for different θ_{ref} sinusoids are visible in Fig.26. Where the blue line represents the bode diagram of the closed loop transfer function. The blue circles represent the identified module and phase from the experimental setup, while the red crosses represent the computed module and phase applying the same sinusoidal references to the non linear simulated system.

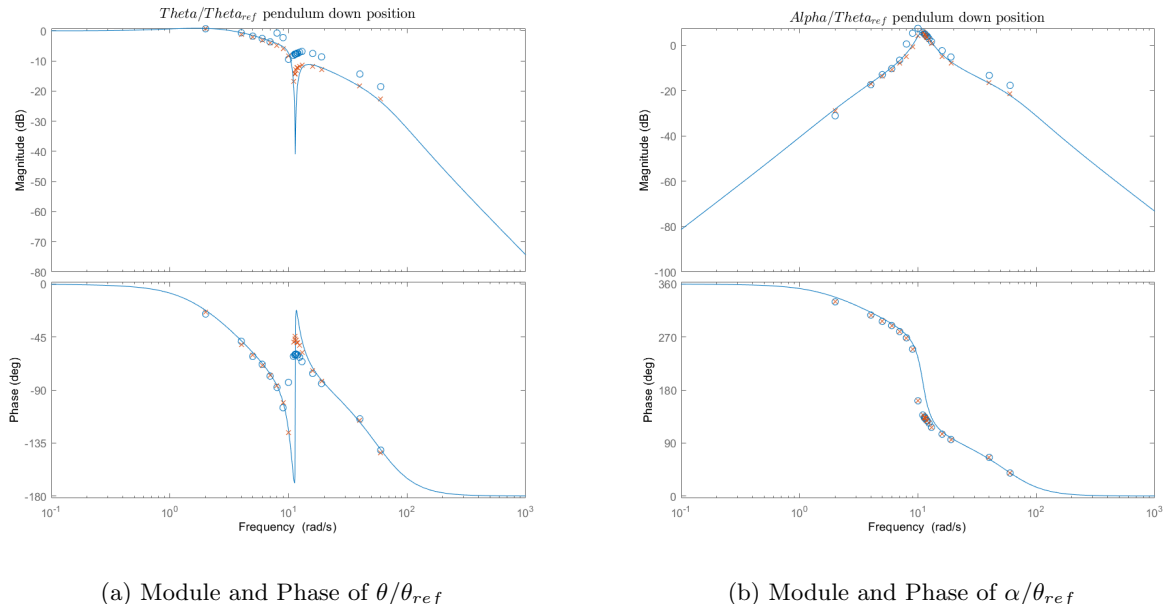


Figure 26: Closed Loop PID Frequency Validation



8 Stabilization of the pendulum in upright position

The aim of this section is to obtain a controller to stabilize the pendulum in the upright position ($\alpha = 180^\circ$).

In order to do so, there are different possible solutions which are commonly composed by a system to observe those states which cannot be measured (i.e. the velocities), and a *State FeedBack Controller*. Here are shown the six options:

- Filtered Derivative Observer + Pole Placement
- Filtered Derivative Observer + Linear Quadratic Regulator
- Luenberger Observer + Pole Placement
- Luenberger Observer + Linear Quadratic Regulator
- Kalman Filter Observer + Pole Placement
- Linear Gaussian Quadratic Regulator (KF + LQR)

8.1 Regulator

8.1.1 Pole Placement

The *Pole Placement method* is used to design a feedback matrix K such that the closed loop system has prescribed eigenvalues.

This is clear looking at this equation:

$$\dot{x}(t) = Ax(t) + Bu(t)$$

And the control law:

$$u(t) = -Kx(t) - \gamma(t)$$

The necessary and sufficient condition for the solution of the pole placement problem is that the pair (A,B) is reachable. Once this is verified it's possible to choose the poles.

The choice here was made by analyzing the poles of the system, then a much faster behaviour is desired so that the chosen vector of the poles has been $-[30, 20, (3.2 + i2.4), (3.2 - i2.4)]$.

The tuning procedure has ended with this vector so as to impose in the dominant poles $\omega_n = 4 \frac{\text{rad}}{\text{s}}$ and $\xi = 0.8$;

$$\xi\omega_n \pm i\omega_n\sqrt{\xi^2 - 1} \quad \xi\omega_n = 3.2 \quad i\omega_n\sqrt{\xi^2 - 1} = i2.4$$

With this choice the dynamic was fast enough to keep the pendulum in the upright configuration with slight oscillations. The result obtained by combining the state equation and the control law is:

$$\dot{x}(t) = (A - BK)x(t) + B\gamma(t)$$

8.1.2 Linear Quadratic Regulator

The *LQR Controller* is a dynamic compensator obtained minimizing a cost function $J(x, u)$ function of the state $x(t)$ and the control action $u(t)$.

$$J(x(\cdot), u(\cdot)) = \int_0^{\infty} (x(\tau)^T Q_{lq} x(\tau) + u(\tau)^T R_{lq} u(\tau)) d\tau$$

The cost function described before uses two diagonal matrices Q_{lq} and R_{lq} to weight the state and the input.

Their values are design parameters chosen by doing some simulation tests: big weights are used for the pendulum angle and the input (voltage) to prioritise the stabilization and avoid a too strong control action. The obtained matrices are:



$$Q_{lq} = \begin{bmatrix} \frac{135^2}{45} & 0 & 0 & 0 \\ 0 & \frac{180*360}{360^2} & 0 & 0 \\ 0 & 0 & \frac{1}{10^2} & 0 \\ 0 & 0 & 0 & \frac{300}{30^2} \end{bmatrix} \quad R_{lq} = \left[\frac{100}{10^2} \right]$$

The other ones have been selected so as to proper select the velocities and to limit the movement of the rod in a certain range.

The following step is to normalize these values to obtain each parameter in the interval [0,1]. This is done so that their choice is independent on the measurement units. The values used have been selected by considering the maximum extension values of the angle velocities and positions. For θ the maximum values evaluated from the real setup has been 135° while for α has been 360° . For the velocities: $\dot{\theta}=10 \text{ rad/s}$ and $\dot{\alpha}=30 \text{ rad/s}$. For R_{lq} its value is normalized with respect to the maximum value of voltage $V = 10V$.

By knowing that $Q_{lq} = C_q^T C_q$ one can obtain the C_q matrix.

Now it's necessary to check if the conditions of controllability of (A, B) and the observability of (A, C_q) are verified. The resulting K matrix is then used to compute the classic block diagram of LQR.

8.2 Observer

8.2.1 Filtered Derivative

A simple, but efficient way, to produce velocity estimation is to filter the angles measurement signals, via Low Pass filter in series with a derivative action. The LP time constant is upper limited by the communication channel rate of $2ms$, while it is lower limited by the open loop bandwidth of $4\frac{\text{rad}}{\text{s}}$. Given this interval the LP pole has been set to $100Hz$, as can be seen in Fig. 27.

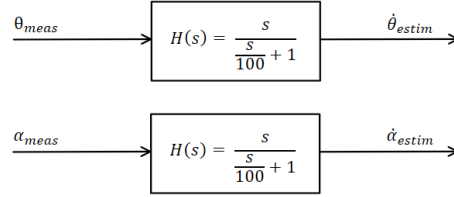


Figure 27: Filtered Derivative

8.2.2 Luenberger Observer

The idea of the observer is to build a system which, based on the input and output measurements, computes an estimate \hat{x} of the system state x . This is clear from these equations:

$$\dot{\hat{x}}(t) = A\hat{x}(t) + Bu(t) + L[y(t) - C\hat{x}(t) - Du(t)]$$

Where L is a design choice.

The $e_y(t)$ is the output estimation error and $e(t)$ the state estimation error:

$$e_y(t) = [y(t) - C\hat{x}(t) - Du(t)]$$

$$e(t) = x(t) - \hat{x}(t)$$



The dynamic of the state estimation error is the following:

$$\dot{e}(t) = (A - LC)e(t)$$

The necessary and sufficient condition for the design of an asymptotic observer is that the pair (A, C) is observable.

The main idea now is to use pole assignment to select the observer gain L to assign the eigenvalues of $(A - LC)$ so that the error tends to zero. To do it a typical choice is to have them much faster than the ones of $(A - BK)$ which are those of the closed loop system with a state feedback control law.

The chosen ones here are: $[-200; -200; -100; -100]$.

8.2.3 Kalman Filter

The *Kalman Filter* is a state observer which shows optimality properties for systems subject to stochastic disturbances. The procedure is similar to the one used for the LQ control.

Starting from the classical system in State Space form, the first condition that must be checked is that the pair (A, B_q) is reachable. B_q is obtained from this relation: $\tilde{Q} = B_q B_q^T$.

The second condition is that (A, C) is observable. Once them are verified it's possible to say that:

- The optimal estimator is:

$$\dot{\hat{x}}(t) = A\hat{x}(t) + Bu(t) + \bar{L}[y(t) - C\hat{x}(t)] = (A - \bar{L}C)\hat{x}(t) + Bu(t) + \bar{L}y(t)$$

- The observer is asymptotically stable: all the eigenvalues of $(A - \bar{L}C)$ have negative real part.

Noise Characterization:

The Measurement Noise covariance can be easily estimated from the Encoder resolution: $res = \frac{2\pi}{2048}$.

$$\tilde{R} = \begin{bmatrix} \left(\frac{res}{2\sqrt{3}}\right)^2 & 0 \\ 0 & \left(\frac{res}{2\sqrt{3}}\right)^2 \end{bmatrix} \approx \begin{bmatrix} 7.84 \cdot 10^{-7} & 0 \\ 0 & 7.84 \cdot 10^{-7} \end{bmatrix}$$

For the estimation of Process noise covariance, the data-based method known in the literature as generative method (4) has been chosen. Exploiting the discrete state space equation of the model:

$$\begin{cases} x(k+1) = F \cdot x(k) + G \cdot u(k) + v_x(k) \\ y(k) = H \cdot x(k) + v_y(k) \end{cases}$$

One can produce a 1-step ahead estimation of the state $\hat{x}(i)$ using the measured state $\tilde{x}(i-1)$ and the measured input $\tilde{u}(i-1)$, and estimate the noise covariance as the covariance of the error between the estimated state $\hat{x}(i)$, and the measured one $\tilde{x}(i)$, in equation:

$$\tilde{Q} = Var[\tilde{x}(t) - \hat{x}(t)] = \frac{1}{N} \sum_{i=0}^N (\tilde{x}(i) - F \cdot \tilde{x}(i-1) - G \cdot \tilde{u}(i-1)) \cdot (\tilde{x}(i) - F \cdot \tilde{x}(i-1) - G \cdot \tilde{u}(i-1))^T$$

Using as measured data the ones from a chirp experiment, with the derivative $\dot{\theta}, \dot{\alpha}$ produced with filtered derivative approach, this is obtained:

$$\tilde{Q} = \begin{bmatrix} 1.83 \cdot 10^{-6} & -3.86 \cdot 10^{-7} & 4.00 \cdot 10^{-5} & -7.38 \cdot 10^{-5} \\ -3.86 \cdot 10^{-7} & 2.40 \cdot 10^{-6} & 1.39 \cdot 10^{-6} & 1.86 \cdot 10^{-4} \\ 4.00 \cdot 10^{-5} & 1.39 \cdot 10^{-6} & 4.28 \cdot 10^{-3} & 7.32 \cdot 10^{-4} \\ -7.38 \cdot 10^{-5} & 1.86 \cdot 10^{-4} & 7.32 \cdot 10^{-4} & 3.31 \cdot 10^{-2} \end{bmatrix}$$

What can be said from the analysis is that considering the values for \tilde{R} and \tilde{Q} , the Kalman filter trusts a lot the measurements on θ and α , while it trusts more the model for the values of $\dot{\theta}$ and $\dot{\alpha}$, as we might expect

from this system in which angle measurements are not so noisy and velocity measurement are not directly available. The Noise covariance estimation led to the realization of the following poles for the error dynamic in the system with Stationary Kalman Filter:

$$\begin{pmatrix} -6.2600 + 7.4266i \\ -6.2600 - 7.4266i \\ -16.8315 + 6.1728i \\ -16.8315 - 6.1728i \end{pmatrix}$$

8.2.4 Comparison between observers

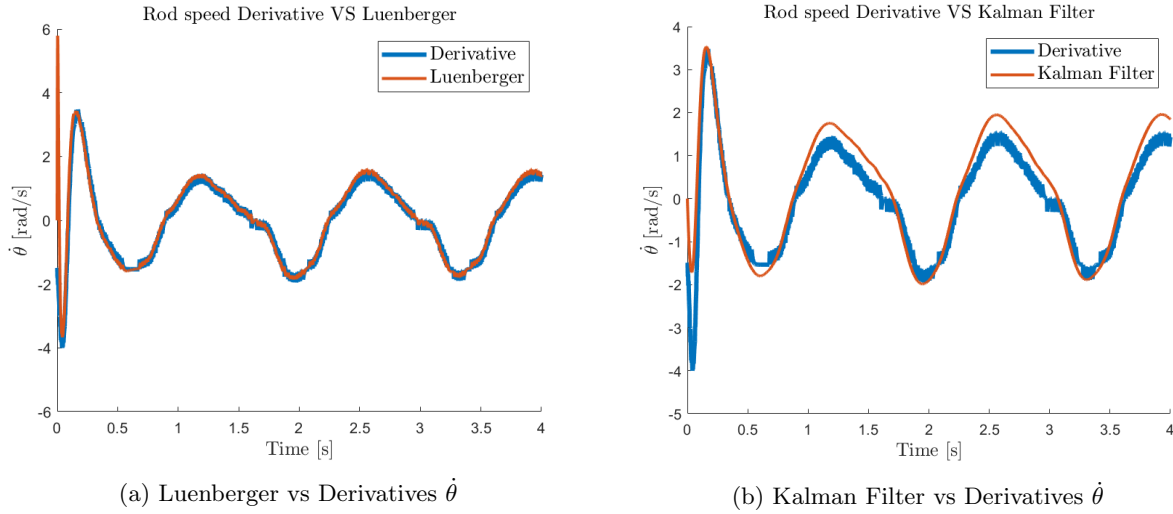


Figure 28: Rod Speed

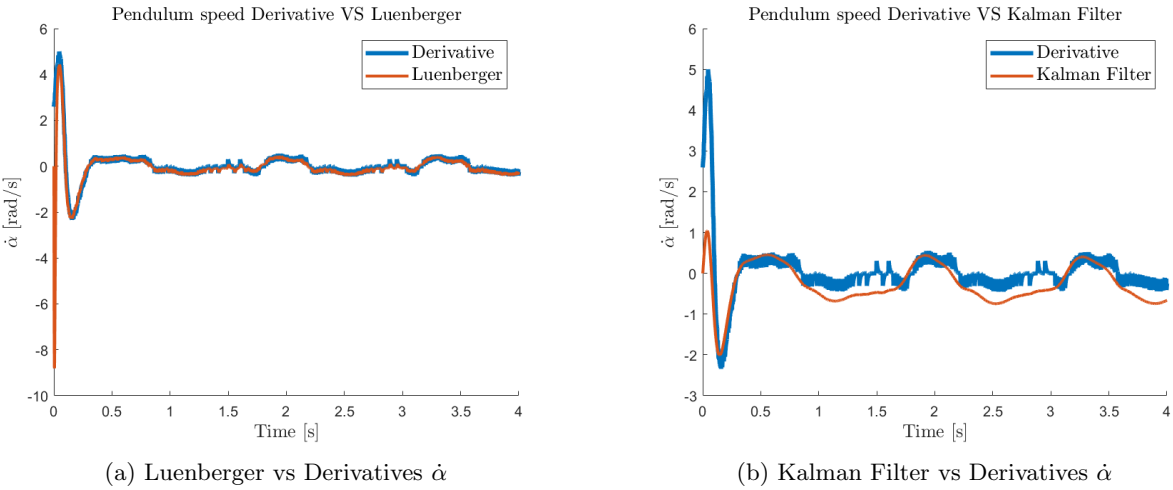


Figure 29: Pendulum Speed

From the comparison plots it's understandable that the Kalman Filter has a bigger convergence time with respect to the Luenberger observer. As a consequence, we will see that when the Kalman Filter is adopted by a control scheme to follow a given reference, the controlled variable will need more time to converge to the desired value. This is verified by the closed-loop poles of the error dynamic when adopting these

observers: the chosen ones for the Luenberger are much faster compared to the ones derived from the noise characterization of the Kalman Filter. Moreover, the dominant poles have:

$$\omega_{nLUN} = 100 \frac{rad}{s} \quad \omega_{nKF} = \sqrt{\Re^2 + \Im^2} \approx 10 \frac{rad}{s}$$

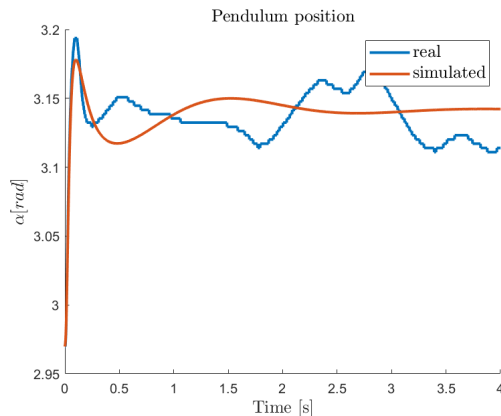
Both the Luenberger and the Kalman Filter are initialised with the pendulum position at the upright position and setting the other states to zero. The reason for this initialization is due to the activation of the stabilizing controller around this point, with a speed that is impossible to know a priori.

This can be seen, in the plot at the beginning of the simulation, where also the time needed by the two observers to reach the estimation, given by the derivatives, can be appreciated.

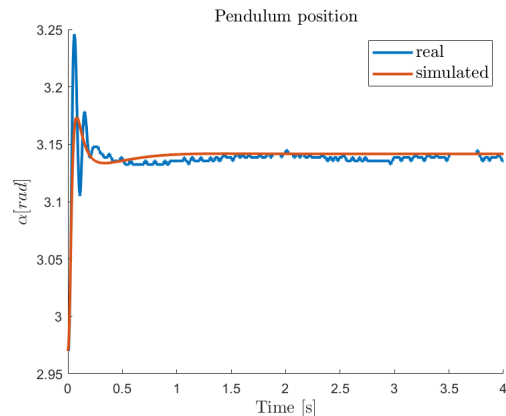
8.3 Final results

Here it's shown the simulation of each type of scheme has been explained before¹:

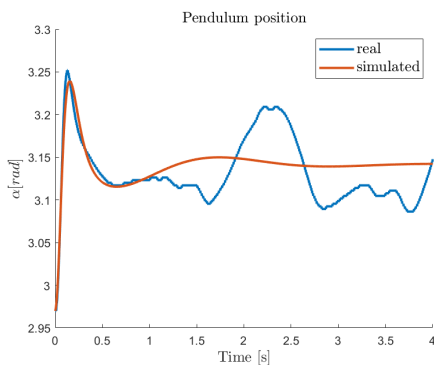
8.3.1 Comparison of α



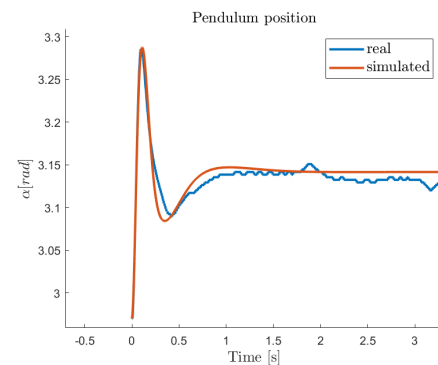
(a) LQR with Luenberger



(b) PP with Luenberger



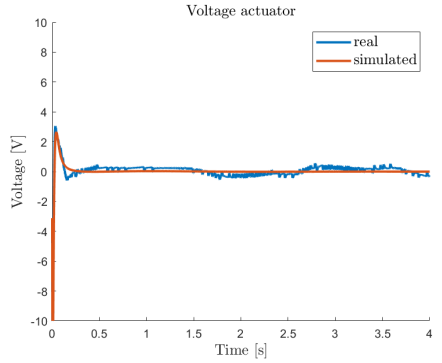
(a) LQR with KF



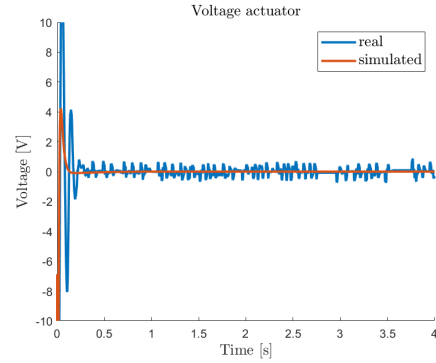
(b) PP with KF

¹The validation in time using derivatives is not reported here because it's very similar to the one adopting the Luenberger observer as it's visible from the comparison plots in section 8.2.4

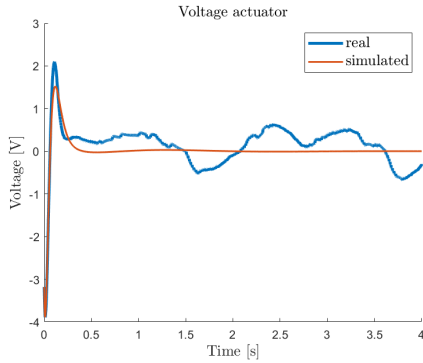
8.3.2 Comparison of V_m



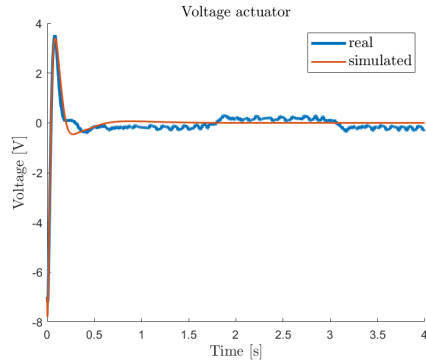
(a) LQR with Luenberger



(b) PP with Luenberger



(a) LQR with KF



(b) PP with KF

From the plots on α it's visible that the *Pole Placement* is faster/more aggressive than the tuned *LQR*. Indeed, using *LQR* there are bigger oscillations on the pendulum's angle. This is confirmed by the closed loop poles which come from the adoption of the *LQR* technique:

$$\begin{pmatrix} -1.0902 + 2.6766i \\ -1.0902 - 2.6766i \\ -9.0871 + 0.0000i \\ -26.8665 + 0.0000i \end{pmatrix}$$

Indeed, the pair of complex conjugate dominant poles here is closer to the imaginary axis with respect to the chosen one for the *Pole Placement* technique resulting in a slower dynamics; moreover:

$$\omega_n = \sqrt{\Re^2 + \Im^2} = 2.89 \frac{\text{rad}}{\text{s}}$$

$$\xi = \frac{\Re}{\omega_n} = 0.4$$

The natural frequency is smaller with respect to the one chosen to tune *Pole Placement* and the damping ratio is smaller, giving a justification to the bigger visible oscillatory behaviour of the *LQR* control. In the end, it has been decided to keep those chosen Q and R matrices for the tuning of *LQR* in order to have a less aggressive controller (i.e. with respect to the one defined for *Pole Placement*) and this is confirmed in the voltage comparison section 8.3.2; despite that it was able to fulfil the goal of keeping the pendulum in the unstable equilibrium position.

Again, the same controller with Luenberger observer and Kalman Filter presents a slower convergence



dynamic on α due to the bigger convergence time needed by the latter observer as already said in section 8.2.4.

The same comments can be made in the comparison of these two techniques when they are enlarged in the next section 9 to also follow a given reference in the horizontal rod angle. This is the case because the desired poles of *Pole Placement* are kept the same with the addition of a fast pole, also the tuning matrices of *LQR* are the same with the addition of a fifth element on the diagonal of Q that gives these closed loop poles:

$$\begin{pmatrix} -1.8962 + 3.9480i \\ -1.8962 - 3.9480i \\ -3.4778 + 0.0000i \\ -9.0871 + 0.0000i \\ -26.8665 + 0.0000i \end{pmatrix}$$

Again the extended *LQR* has a behavior similar to the not extended case. In that section the bigger oscillatory behavior of *LQR* and the higher convergence time required by KF is also visible in θ .

9 Position control and stabilization in upright configuration

The aim of this section is to show the combined control of the horizontal arm while stabilizing the pendulum in the upright position.

9.1 Extended Pole Placement

Maintaining the same structure described before the state of the system has been extended by adding an integrator dynamic on θ so as to guarantee zero steady state error between reference and measurement; the corresponding pole has been chosen to be placed at: [-20].

In the result section the configurations with Luenberger Observer and Kalman Filter are shown.

9.2 Extended LQR

The second chosen control scheme has been the *LQR* one with integral action: starting from the linearized system in state space form, again as done for the *pole placement* the state of the system is extended by adding an integrator dynamic on θ to have zero steady state error.

As described before, the weights have been chosen by doing some simulation tests. The new Q_{lq} is a [5x5] matrix equal to the previous one but with a new term in the 5th row. This term is due to the integral action and its role is to control the horizontal arm to the desired position. The weight of this term is big so as to obtain a good reference tracking of θ_{ref} .

The new matrices are now:

$$Q_{lq} = \begin{bmatrix} \frac{135^2}{45} & 0 & 0 & 0 & 0 \\ \frac{135^2}{45} & 0 & 0 & 0 & 0 \\ 0 & \frac{180*360}{360^2} & 0 & 0 & 0 \\ 0 & 0 & \frac{1}{10^2} & 0 & 0 \\ 0 & 0 & 0 & \frac{300}{30^2} & 0 \\ 0 & 0 & 0 & 0 & 20 \end{bmatrix} \quad R_{lq} = \left[\frac{100}{10^2} \right]$$

9.3 Frequency validation

The frequency validation with the same technique described in section 7 has been performed with the following depicted bodes on:

1. extended LQR with derivatives.
2. extended PP with Leunberger observer.
3. extended PP with Kalman Filter.
4. extended LQR with Kalman Filter.

Some of the options explained above have not been reported because as written here in above, the derivatives and the Luenberger observer provide very similar results. Therefore the frequency validation of PP with derivatives is not reported as its plots are very close to those of PP with Luenberger observer, the same for the validation of LQR with Luenberger as it has already been reported the one with the filtered derivatives.

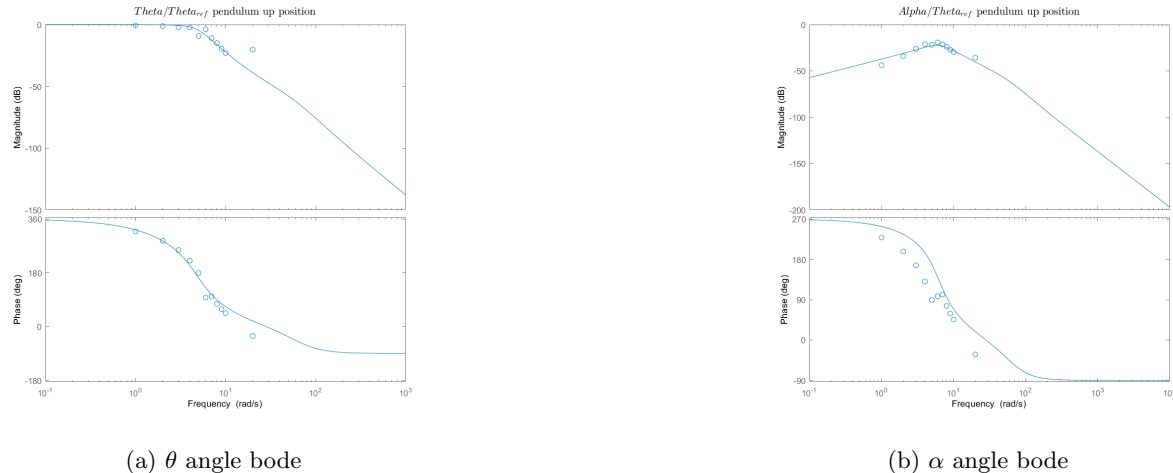


Figure 34: extended LQR with derivatives

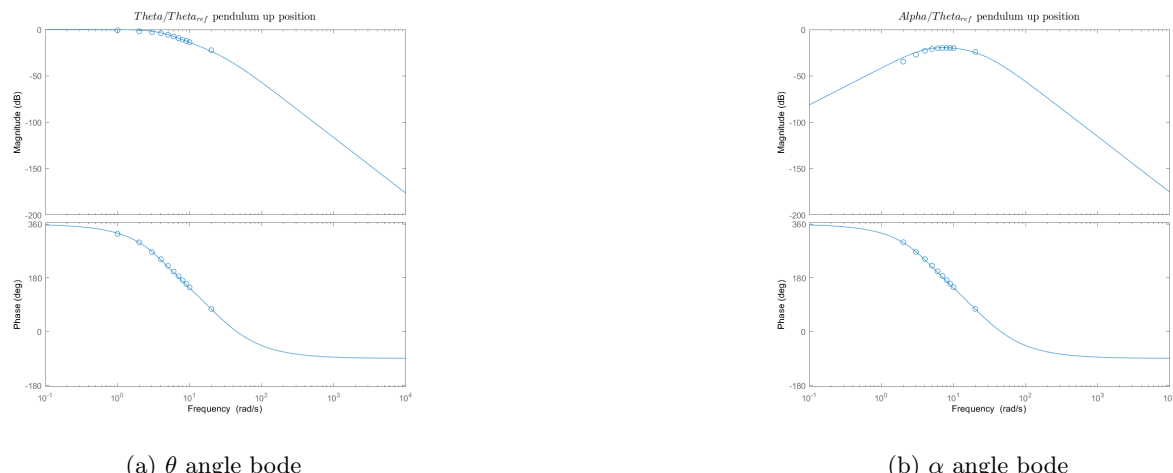


Figure 35: extended PP with Luenberger

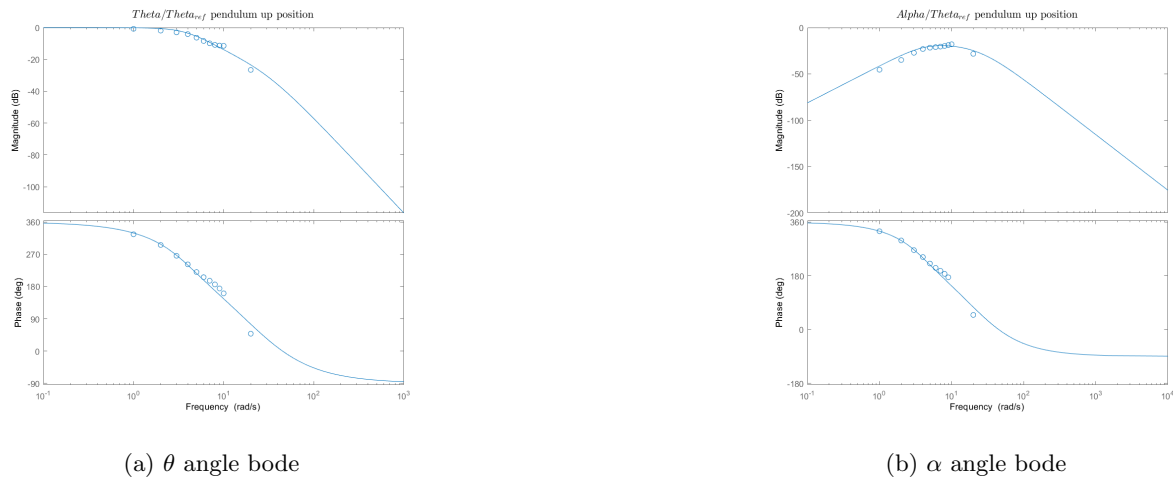


Figure 36: extended PP with Kalman Filter

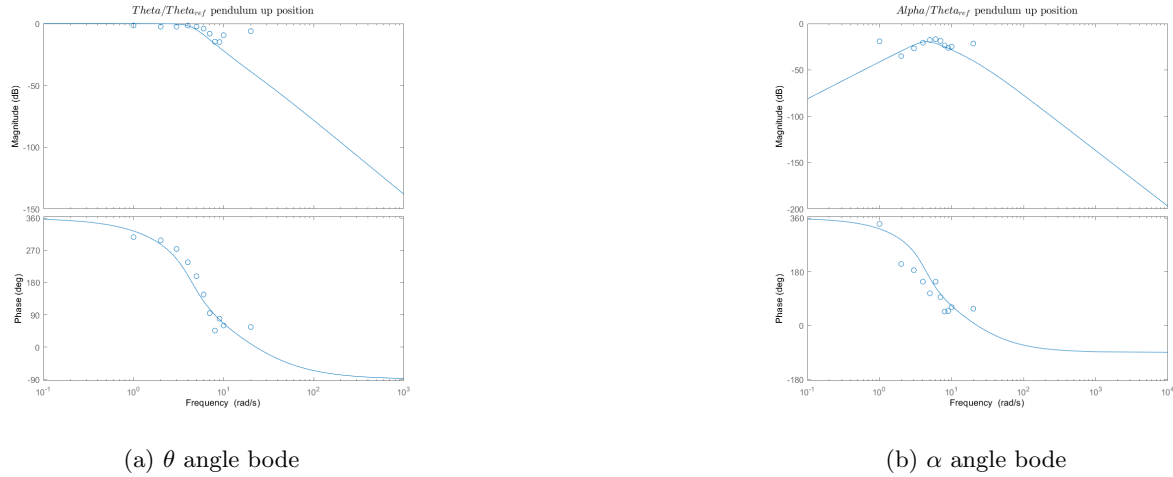
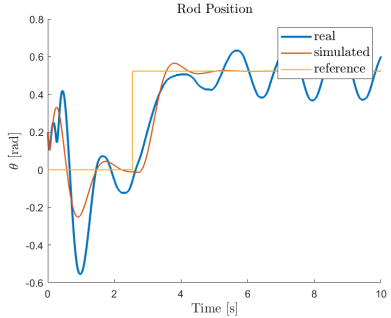


Figure 37: extended LQR with Kalman Filter

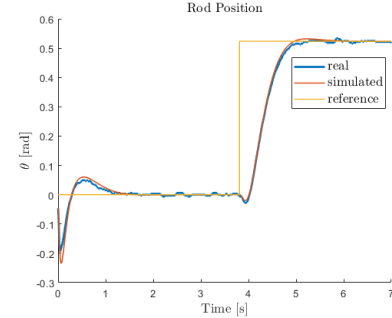
In the result section the configurations with Luenberger Observer and Kalman Filter are shown, while the configuration with derivatives is not reported for the reason detailed in the footnote above¹.

9.4 Results comparison

9.4.1 Comparison of θ

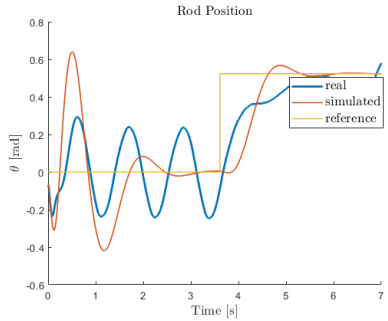


(a) Position Control with LQR with Luenberger

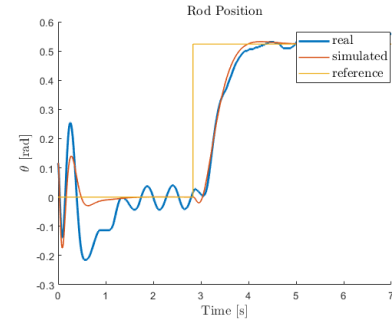


(b) Position Control with PP with Luenberger

Figure 38: Position Control LQR and PP with Luenberger $\theta_{ref} = \frac{\pi}{6}$ rad



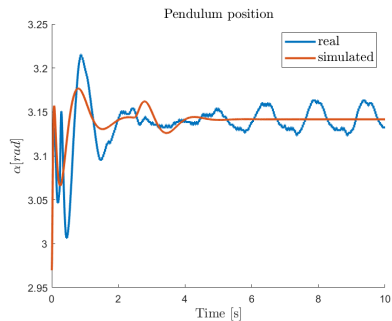
(a) Position Control with LQR with KF



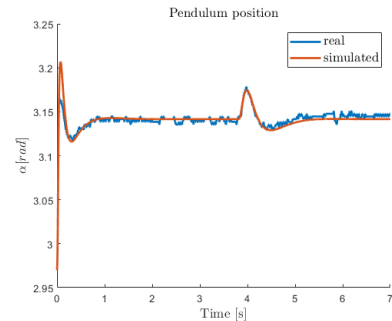
(b) Position Control with PP with KF

Figure 39: Position Control LQR/PP with KF $\theta_{ref} = \frac{\pi}{6}$ rad

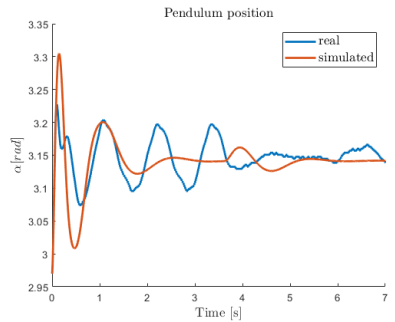
9.4.2 Comparison of α



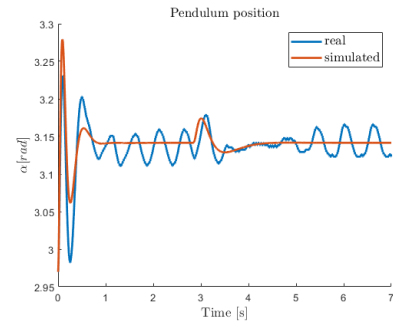
(a) Upright position with LQR with Luenberger



(b) Upright position with PP with Luenberger



(a) Upright position with LQR with KF

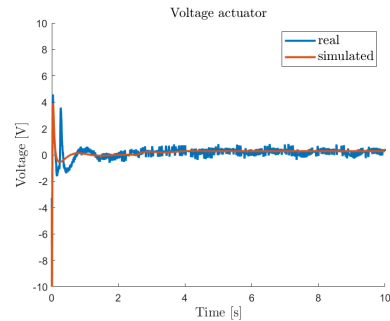


(b) Upright position with PP with KF

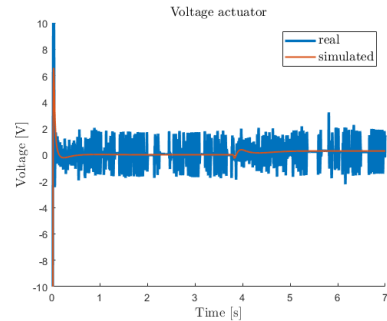
In the above section 9.4.2 it can be noticed the effect of the step reference θ_{ref} on the pendulum. Indeed, one can see a perturbation in the α trajectory due to this change.

Nevertheless, the pendulum stabilization is guaranteed with all the described controller configurations.

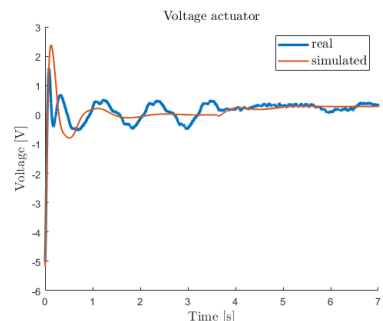
9.4.3 Comparison of Vm



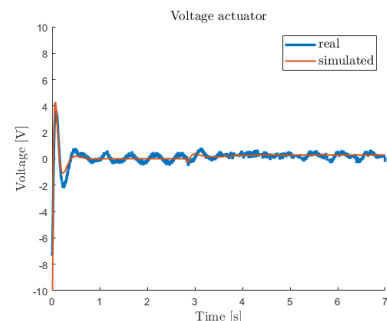
(a) Voltage with LQR with Luenberger



(b) Voltage with PP with Luenberger



(a) Voltage with LQR with KF

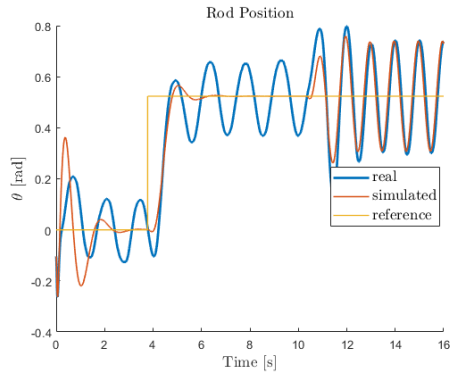


(b) Voltage with PP with KF

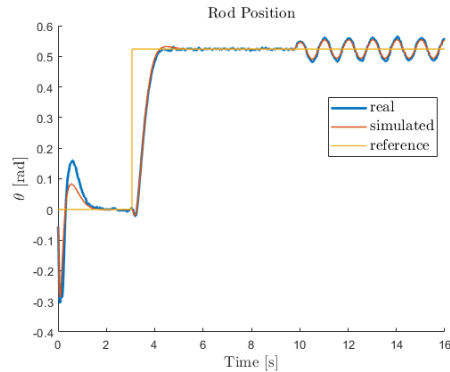
A side note to remark that the Pole Placement scheme with Luenberger observer is the fastest one but this aggressiveness clearly shows off in the voltage trembling between higher values compared to other schemes. On the other hand, in the LQR scheme with Kalman filter the voltage is smooth being this scheme the slowest one.

9.5 Robustness test

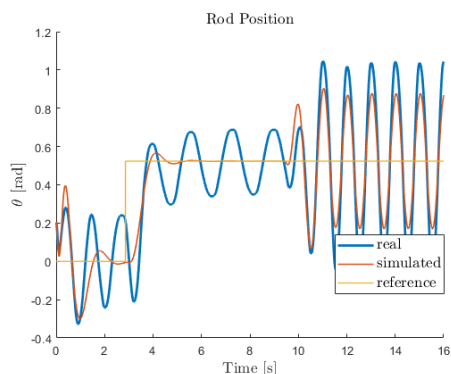
It has been tested also the robustness of each scheme while following a $\theta_{ref} = \frac{\pi}{6}$ rad, with respect to a disturbance sine signal entering at 10 seconds with a frequency of 1Hz and amplitude 0.3 rad. From the results reported below it's visible that all schemes can still perform their reference goal of θ_{ref} while keeping the pendulum in the upright position. Again, the speed of the Luenberger observer compared to the Kalman filter and the aggressiveness of the Pole Placement controller with respect to the LQR are clearly visible in the oscillations of θ while it tracks the step. In addition, the bigger convergence time of Kalman Filter is tangible in the higher oscillations for the same controller when it's equipped with Luenberger observer and when it has the Kalman Filter.



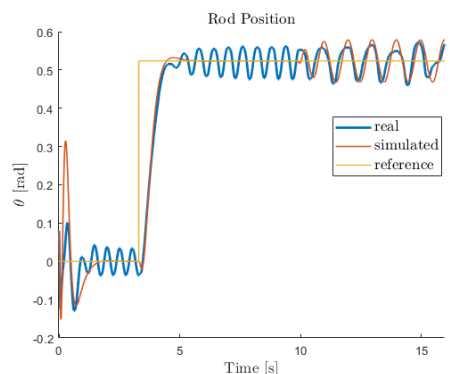
(a) Position Control with LQR with Luenberger



(b) Position Control with PP with Luenberger



(a) Position Control with LQR with Kalman Filter



(b) Position Control with PP with Kalman Filter

9.6 Comments

To obtain better tracking performance in following θ_{ref} it's possible to substitute the integral action on the error provided by the extended LQR or PP with a full PID control (i.e. the one from the position control of θ in section 6) and a non extended LQR or PP. In this way, we also have the benefits brought by the derivative and proportional action and the horizontal rod is able to follow more dynamic references while keeping the pendulum in the upright position. As a proof, it is shown the results and validation in time of PP with PID using derivatives in Fig. 46.

This experiment is another proof that the designed *Pole Placement* is more “aggressive/faster” than the tuned *LQR* control and it can track highly varying reference signals while keeping the vertical rod in the desired position. As a matter of fact, the same experiment was conducted with LQR in place of PP and after some time, when the reference signal dynamic was increasing, the LQR was no more able to keep the

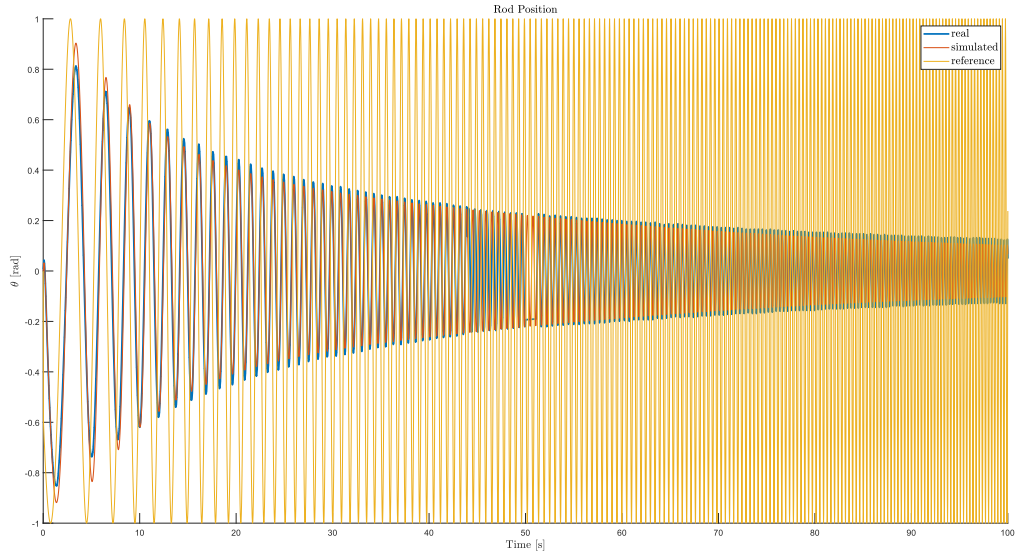


Figure 46: θ with θ_{ref} a chirp signal

pendulum in the upright position and it fell down. This is due to the conflict of interest in the control action to achieve the two different goals; indeed, the PID wants to track the reference disregarding the stabilization in the upright position of the pendulum. A different design of the LQR should be done giving higher priority to θ , α while giving more freedom to $\dot{\theta}$, $\dot{\alpha}$ and the voltage V_m .

10 Swing up

The aim of this section is to show an advanced control scheme able to swing up the pendulum in the upright position starting from the stable equilibrium $\alpha = 0^\circ$.

The one shown here is the *Energy Based Lyapunov Method*: the idea of energy control is based on the preservation of energy in ideal systems(i.e. the sum of kinetic and potential energy is constant).

Two important initial hypotheses have been: neglecting the term multiplied by the square of $\dot{\theta}$ in the model equations and considering a zero viscous friction force because friction will be damping the oscillation in practice and the overall system energy will not be constant.

Starting from the dynamic equations of the pendulum (the second one described in the [equation](#) model), the chosen control action is $\ddot{\theta} = u$.

$$\ddot{\theta} = u$$

By substituting this in the mentioned equation it becomes:

$$(m_p l_p^2 + J_p) \ddot{\alpha}^2 + m_p l_p g \sin \alpha + m_p l_2 \cos \alpha L_r u = 0 \quad (2)$$

Following the theory of this method a positive definite Lyapunov function has been chosen:

$$V = \frac{1}{2}(E - E_D)^2$$

So that:

$$\dot{V} = \dot{E}(E - E_D)$$

Where E_D is the desired energy in the upright position where there is only the potential term which is zero because the design choice has been set so as to consider zero potential in this position.

The other term is the total energy of the pendulum which follows this relation:

$$E = \frac{1}{2}(m_p l_p^2 + J_p) \dot{\alpha}^2 + m_p l_p g(1 - \cos\alpha)$$

So that:

$$\dot{E} = -m_p l_p \cos\alpha \dot{\alpha} L_r u$$

Obtained by substitution of the $\ddot{\alpha}$ term from (2).

Now, these terms are substituted in the \dot{V} equation:

$$\dot{V} = -(E - E_D)m_p l_p \cos\alpha \dot{\alpha} L_r u$$

It is possible to control the energy of the pendulum with the non linear control law:

$$u = (E - E_D)\dot{\alpha} \cos\alpha$$

With this control action the Lyapunov function \dot{V} is always semi-definite negative.

For the system energy to change quickly, the magnitude of the control signal must be large. As a result the following swing-up control is implemented in the controller as:

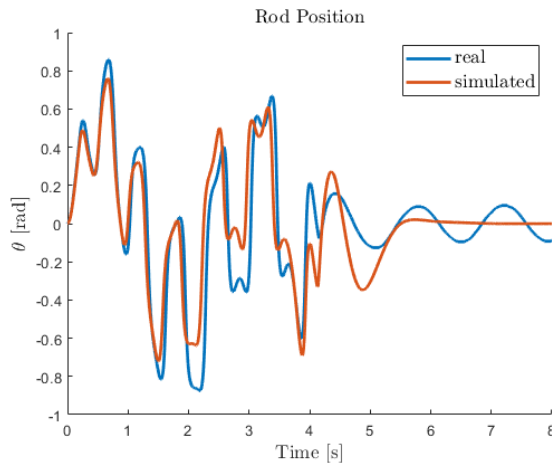
$$u = K(E - E_D)\text{sign}(\dot{\alpha} \cos\alpha)$$

Where the *sign* operator is used to enable faster control switching (the motor gives the steep change in the θ angle when the pendulum has no kinetic energy so $\dot{\alpha} = 0$ and it's going to change its oscillatory direction) and K is simply a gain through which is possible to decide the aggressiveness of the horizontal rod; in other words, the bigger K is, the lower the number of oscillations needed by the rod to bring the pendulum in the upright position. K was chosen equal to 30.

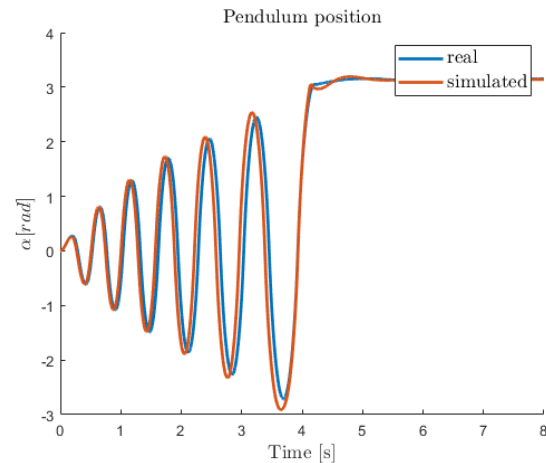
10.1 Switching system and results

The switching system is designed to activate the LQR control once the pendulum angle is around $\pm 10^\circ$ the upright position.

Moreover, the overall Swing Up controller is able to deal with the periodicity of the pendulum angle. The results obtained with the above explained advanced control to achieve the goal of the *swing up* with derivatives are shown below.



(a) Swing up: evolution of θ



(b) Swing up: evolution of α

These plots represent the in-lab simulation with the expected simulation given by the realised Simulink model.



It can be noticed how the simulation matches the real setup in the first seconds and then slightly changes, especially in the rod position.

This happens because the identification procedure is realized on an experiment with limited oscillation of the pendulum and not in an experiment where a full round of the angle is experienced.

Moreover this difference can be inferred by a simple model of the friction and of the encoder cable stiffness.

11 Extended Kalman Filter

The Extended Kalman Filter used in this work is noted in the literature as ***Continuous Extended Kalman Filter with discrete measurements***(3).

The logic behind this scheme (Fig.48) is that the state evolution happens in continuous time using the non linear dynamic model, while the EKF update step happens in discrete time using the linearized model around the current state. Similarly as done in section 3, it's possible to linearize the complete dynamic model shown

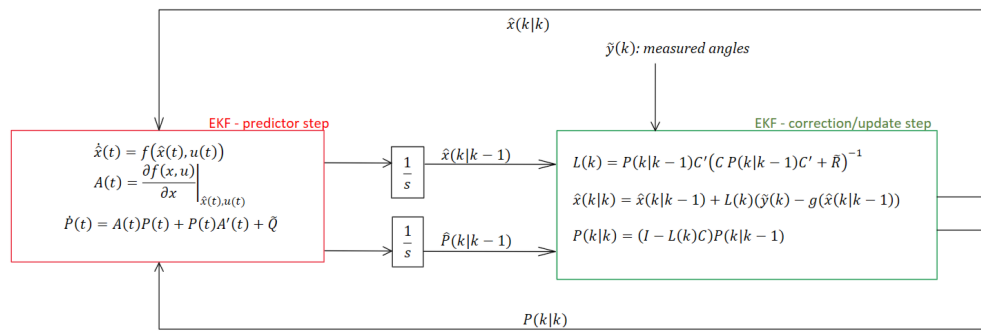


Figure 48: Extended Kalman Filter scheme

in section 2.2. Denoting as $\frac{\partial 1}{\partial x}$ the partial derivative of the first equation with respect the generic variable x , and as $\frac{\partial 2}{\partial x}$ the partial derivative of the second equation with respect the generic variable x . Moreover, defining as:

$$\begin{aligned}
 P1 &= \frac{\partial 1}{\partial \theta} - \frac{\partial 1}{\partial \ddot{\alpha}} \cdot \frac{1}{\frac{\partial 2}{\partial \ddot{\alpha}}} \cdot \frac{\partial 2}{\partial \theta} & P2 &= \frac{\partial 1}{\partial \theta} - \frac{\partial 1}{\partial \ddot{\alpha}} \cdot \frac{1}{\frac{\partial 2}{\partial \ddot{\alpha}}} \cdot \frac{\partial 2}{\partial \theta} & P3 &= \frac{\partial 1}{\partial \theta} - \frac{\partial 1}{\partial \ddot{\alpha}} \cdot \frac{1}{\frac{\partial 2}{\partial \ddot{\alpha}}} \cdot \frac{\partial 2}{\partial \theta} \\
 P4 &= \frac{\partial 1}{\partial \dot{\alpha}} - \frac{\partial 1}{\partial \ddot{\alpha}} \cdot \frac{1}{\frac{\partial 2}{\partial \ddot{\alpha}}} \cdot \frac{\partial 2}{\partial \dot{\alpha}} & P5 &= \frac{\partial 1}{\partial \alpha} + \frac{1}{\frac{\partial 2}{\partial \ddot{\alpha}}} \cdot \frac{\partial 2}{\partial \theta} \cdot \frac{\partial 2}{\partial \alpha} & P6 &= -\frac{\partial 2}{\partial \theta} + \frac{1}{\frac{\partial 2}{\partial \ddot{\alpha}}} \cdot \frac{\partial 2}{\partial \theta} \cdot \frac{P2}{P1} \\
 P7 &= -\frac{\partial 2}{\partial \theta} + \frac{1}{\frac{\partial 2}{\partial \ddot{\alpha}}} \cdot \frac{\partial 2}{\partial \theta} \cdot \frac{P3}{P1} & P8 &= -\frac{\partial 2}{\partial \dot{\alpha}} + \frac{1}{\frac{\partial 2}{\partial \ddot{\alpha}}} \cdot \frac{\partial 2}{\partial \theta} \cdot \frac{P4}{P1} & P9 &= -\frac{\partial 2}{\partial \alpha} + \frac{\partial 1}{\partial \ddot{\alpha}} \cdot \frac{1}{\frac{\partial 2}{\partial \ddot{\alpha}}} \cdot \frac{P5}{P1} \\
 A &= \begin{bmatrix} 0 & 0 & 1 & 0 \\ 0 & 0 & 0 & 1 \\ \frac{P3}{P1} & \frac{P5}{P1} & \frac{P2}{P1} & \frac{P4}{P1} \\ P7 & P9 & P6 & P8 \end{bmatrix}
 \end{aligned}$$

The process noise can be estimated in the same way as done in section 8.2.3, using the non linear model to produce the 1-step ahead estimation instead of the linear one, in equation is:

$$\tilde{Q} = \text{Var} [\tilde{x}(t) - \hat{x}(t)] = \frac{1}{N} \sum_{i=0}^N (\tilde{x}(i) - f(\tilde{x}(i-1), \tilde{u}(i-1))) \cdot (\tilde{x}(i) - f(\tilde{x}(i-1), \tilde{u}(i-1)))^T$$

While the measurement noise covariance matrix \tilde{R} has been left the same as the one of the Kalman Filter. Using as data set one that the simulated model does not fit as well as a chirp, in particular a voltage constructed as sine wave at the resonance frequency followed by a Sawtooth wave at lower frequency, it's possible to obtain a matrix \tilde{Q} such that the resulting Kalman Filter is overall faster. That's because the model error accounted by the process covariance estimation will be greater. Obtaining:

$$\tilde{Q} = \begin{bmatrix} 2.90 \cdot 10^{-6} & -2.21 \cdot 10^{-6} & 5.21 \cdot 10^{-5} & 5.17 \cdot 10^{-6} \\ -2.21 \cdot 10^{-6} & 5.89 \cdot 10^{-6} & -2.20 \cdot 10^{-5} & 2.44 \cdot 10^{-4} \\ 5.21 \cdot 10^{-5} & -2.20 \cdot 10^{-5} & 5.20 \cdot 10^{-3} & -1.70 \cdot 10^{-3} \\ 5.17 \cdot 10^{-6} & 2.44 \cdot 10^{-5} & -1.70 \cdot 10^{-3} & 6.60 \cdot 10^{-3} \end{bmatrix}$$

The other observers defined in the previous sections are constructed using the linearized system around the upright equilibrium, so they do only work around that equilibrium position. Given the working principle of the EKF, this observer scheme has the advantage that it can be used in every working condition and for this motivation it's suitable to be used at every step in the swing up control scheme (both energy control and stabilization). Furthermore, Kalman filters are really sensible to wrong initial conditions, but this problem is not relevant if you use an extended Kalman filter since the initial conditions of the observer can be set to the real one in which all states are zero. This can't be done while using a normal Kalman filter constructed on the linearized model around the upright equilibrium position, since it is activated when it is near this equilibrium position, but with an erroneous initialization (i.e initialized at state upright still, but activated in the range $170^\circ < \alpha < 180^\circ$ with non null velocities). Given the value of \tilde{Q} and \tilde{R} , as expected, it's possible to see (Fig 49) that since the observer trusts a lot the encoder measurements, the estimation of the angles will coincide. This can be furthermore explained looking at the EKF realization: the EKF correction step will align the prediction on the angles (first two states) with the received measurements, ensuring consistency with the real pendulum behaviour.

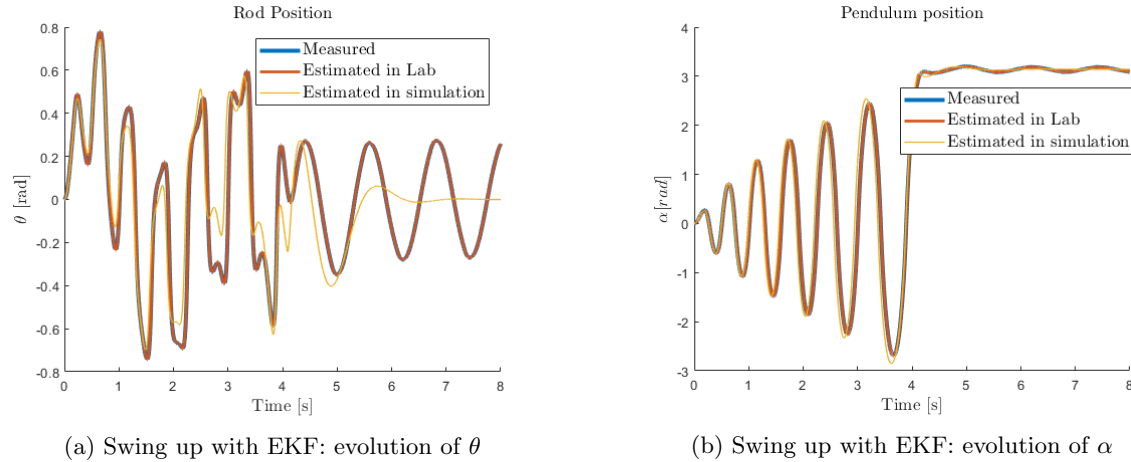


Figure 49

While regarding the angular velocities the EKF has no alternative except trusting the non-linear model prediction, leading to a correct estimation of the velocities when compared to the estimation returned via high pass derivative filter (Fig 50).

12 Finite Horizon Optimal Control Problem

The problem of swinging up the pendulum in its upright position can be treated as an optimization problem where the objective is to bring the pendulum angle to its upright position (i.e $\alpha_{ref} = 180^\circ$) in a fixed amount of time, hence the name *Finite Horizon Optimal Control Problem*, from now on abbreviated as **FHOCP**. By solving the optimization problem is possible to obtain an optimized sequence that can be fed at the setup in open loop to make it swing up. Now let's delve into its mathematical formulation:

$$\vec{V}_m = V_m(0), \dots, V_m(N)$$

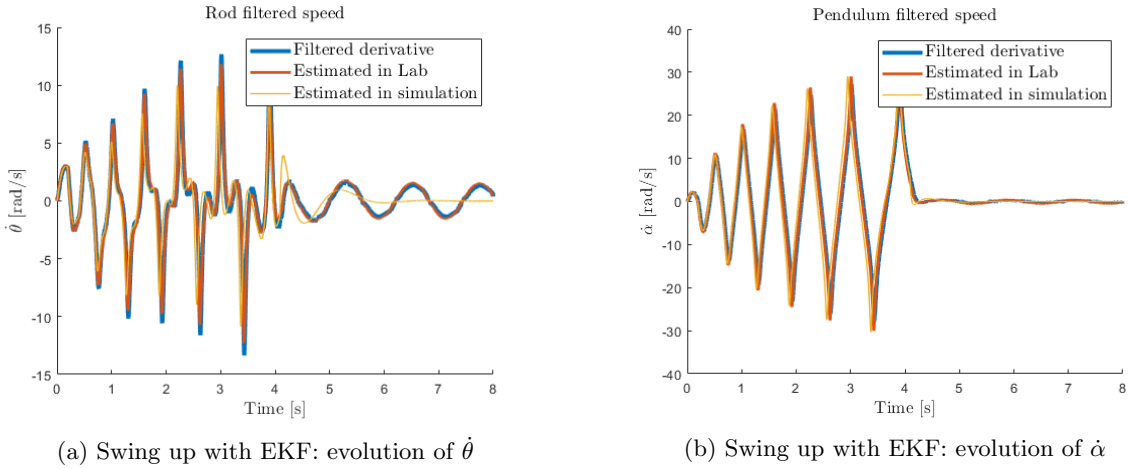


Figure 50

$$\begin{aligned}
 \min_{\vec{V}_m} \quad & \underbrace{\sum_{i=0}^N (\alpha_{ref} - \alpha_{sim}(i))^2 + (\theta_{ref} - \theta_{sim}(i))^2}_{\text{Tracking cost}} + \underbrace{\sum_{i=0}^N 10 \cdot V_m(i)^2}_{\text{Consumption cost}} + \underbrace{10000 \cdot (\alpha_{ref} - \alpha_{sim}(N))^2 + 10 \cdot (\theta_{ref} - \theta_{sim}(N))^2}_{\text{Terminal cost}} \\
 \text{s.t.} \quad & \ddot{q} = B(q, \pi)^{-1} (\tau(v_{meas}(i)) - C(q, \dot{q}, \pi) - B_v(\pi) \dot{q} - K(\pi)(q - q_0) - g(q, \pi)), \\
 & -10V \leq V_m(i) \leq 10V \quad i = 0 \dots N, \\
 & -120^\circ \leq \theta(i) \leq 120^\circ \quad i = 0 \dots N
 \end{aligned}$$

The cost function has been constructed to weight the overall trajectory to bring the pendulum up as fast as possible, while weighting a lot the terminal position to ensure that at the end of the horizon the pendulum will be at the reference $\theta_{ref} = 0$, $\alpha_{ref} = 180^\circ$. At the same time also the input has been weighted to make the generated optimal input smoother and less aggressive. Adopting this control strategy has different advantages(+) and disadvantages(-):

- + It's possible to choose the maximum input usage.
- + It's possible to choose in how much time the pendulum must swing up.
- + It's possible to impose that the angle θ must stay in a prefixed interval.
- This control strategy relies on the fact that the model must be as exact as possible (i.e high fitting in frequency and time), even a small error on the model will make this strategy unfeasible.
- Since the optimization problem is performed offline, it's not possible to react to disturbances or any other unexpected event not taken into account in the FHOCP.
- + It's possible to re-perform the swing up even if it fails some time, or after it has fallen, simply combining this strategy, with a supervisory control that activates a position controller to bring the pendulum in $\alpha = 0^\circ$, $\theta = 0^\circ$, then use the optimized sequence to bring up the pendulum.
- It must be used in combination with a stabilizing controller like LQR or PP that stabilizes the pendulum in its upright configuration once the swing up has been performed via FHOCP.
- + It's possible to weight also the velocities in the cost function to reduce them in the overall optimized trajectory.
- Being a Non-Linear optimization problem is slow and subject to local minima.

Note that most of these problems can be solved adopting a Model Predictive Control working with the same linearized model used for the Extended Kalman Filter (linearized around the trajectory), that achieves real time performance, unlike Non Linear MPC which wouldn't be able to perform the optimization in few milliseconds as required in our setup, thanks to that it can be used as online controller, also to stabilize the pendulum.

The following results are for the optimization problem formulated in this section, where the time horizon has been chosen to be 5 s. The optimized sequence is able to bring the pendulum up. The $\theta_{ref} = 0^\circ$ has not been reached since the weight on the vertical angle is much bigger and the optimized sequence might be stuck on a local minima, which however is satisfying, being the principal objective of this controller to swing up the pendulum while satisfying certain constraints. Note: the terminal position can be enforced through a constraint, but it has been decided to not apply this constraint to make the problem simpler to solve. Furthermore to make the optimization problem much faster to solve the optimized voltage has been down sampled to not make it change every time step, but every 10 time steps, resulting in a lower number of optimization variables, this is visible in Fig.51.

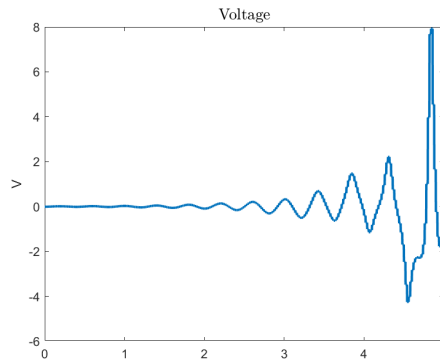


Figure 51: FHOCP optimized voltage

Looking at the plots (Fig. 52) it can be said that the objectives and all constraints are satisfied. Notice that the FHOCP only deals with the swing-up part while the stabilization is left to the stabilizing controller; in this section, LQR in combination with filtered derivative has been used.

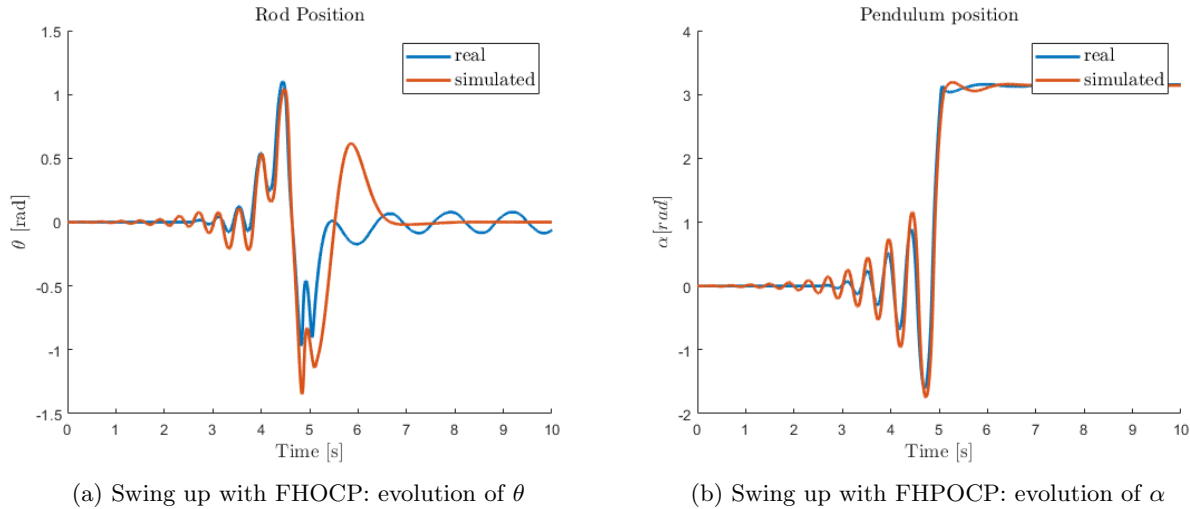


Figure 52



13 Appendix

Symbol	Name	Value	Unit of Measure
m_r	Rod mass	$9.5 \cdot 10^{-2}$	kg
m_p	Pendulum mass	$2.4 \cdot 10^{-2}$	kg
L_r	Length of horizontal arm	$8.5 \cdot 10^{-2}$	m
L_p	Length of pendulum	$1.29 \cdot 10^{-1}$	m
l_r	Length of horizontal arm to c.o.m.	$2.61 \cdot 10^{-2}$	m
l_p	Length of pendulum to c.o.m.	$6.45 \cdot 10^{-2}$	m
J_r	Moment of inertia of horizontal arm about its c.o.m.	$8.27 \cdot 10^{-5}$	$Kg \cdot m^2$
J_p	Moment of inertia of pendulum about its c.o.m.	$1.65 \cdot 10^{-5}$	$Kg \cdot m^2$
J_m	Moment of inertia of motor rotor about its c.o.m.	$6.34 \cdot 10^{-6}$	$Kg \cdot m^2$
J_m	Moment of inertia of attachment hub about its c.o.m.	$9.48 \cdot 10^{-7}$	$Kg \cdot m^2$
B_r	first rotational joint viscous damping	$1.95 \cdot 10^{-4}$	$N \cdot m \cdot s \cdot rad^{-1}$
B_p	Second rotational joint viscous damping	$6.84 \cdot 10^{-6}$	$N \cdot m \cdot s \cdot rad^{-1}$
K_s	Torsional spring stiffness	$2.6 \cdot 10^{-3}$	$N \cdot m \cdot rad^{-1}$
g_0	Gravitational acceleration	9.81	$m \cdot s^{-2}$
$\tau_{s\theta}$	Static friction of first link	$9.61 \cdot 10^{-4}$	$N \cdot m$
R_m	Terminal resistance	8.4	Ω
K_m	Motor back-emf constant	$4.2 \cdot 10^{-2}$	$V \cdot s \cdot rad^{-1}$
K_t	Motor torque constant	$4.2 \cdot 10^{-2}$	$N \cdot m \cdot A^{-1}$
L_m	Rotor inductance	$1.16 \cdot 10^{-3}$	H
V_{sat}	Saturation voltage	10	V
T_s	Sampling time	$2 \cdot 10^{-3}$	S

Table 1: Model parameters

Symbol	Name	Unit of measure
$\theta(t)$	Angular position of horizontal arm	rad
$\dot{\theta}(t)$	Angular velocity of horizontal arm	$rad \cdot s^{-1}$
$\ddot{\theta}(t)$	Angular acceleration of horizontal arm	$rad \cdot s^{-2}$
$\alpha(t)$	Angular position of pendulum	rad
$\dot{\alpha}(t)$	Angular velocity of pendulum	$rad \cdot s^{-1}$
$\ddot{\alpha}(t)$	Angular acceleration of pendulum	$rad \cdot s^{-2}$
$V_m(t)$	input voltage	V
$q(t)$	State Vector	

Table 2: List of symbols



References

- [1] Cazzolato B.S., Prime Z. *On the Dynamics of the Furuta Pendulum. Journal of Control Science and Engineering.* 2011; 2011(6):1–8.
- [2] Räsänen T., Pyrhönen V.P. *State feedback control of a rotary inverted pendulum.* In E. Juuso (Ed.), Automaatiopäivät 23: (2019), Oulu Suomen Automaatioseura.
- [3] Magni L., Scattolini R. *Advance and multivariable control.* Pitagora Editrice Bologna, 2020.
- [4] Dr Barak Or. *tuning-q-matrix-for-cv-and-ca-models-in-kalman-filter.* towardsdatascience.com.
- [5] Bolzern P., Scattolini R., Schiavoni N. *Fondamenti di controlli automatici.* McGraw-Hill, IV edizione 2015.
- [6] Åström K.J., Furuta K., *Swinging up a pendulum by energy control,* Automatica, Volume 36, Issue 2, 2000, pages 287-295.